

¹ Simultaneous SNP selection and adjustment for
² population structure in high dimensional prediction
³ models

⁴ Sahir R Bhatnagar^{1,2}, Yi Yang⁴, Tianyuan Lu², Erwin Schurr⁶,
⁵ JC Loredo-Osti⁷, Marie Forest², Karim Oualkacha³, and
⁶ Celia MT Greenwood^{1,2,5}

⁷ ¹Department of Epidemiology, Biostatistics and Occupational Health, McGill
⁸ University

⁹ ²Lady Davis Institute, Jewish General Hospital, Montréal, QC

¹⁰ ³Département de Mathématiques, Université de Québec à Montréal

¹¹ ⁴Department of Mathematics and Statistics, McGill University

¹² ⁵Departments of Oncology and Human Genetics, McGill University

¹³ ⁶Department of Medicine, McGill University

¹⁴ ⁷Department of Mathematics and Statistics, Memorial University

¹⁵ March 9, 2020

¹⁶ **Abstract**

¹⁷ Complex traits are known to be influenced by a combination of environmental fac-

18 tors and rare and common genetic variants. However, detection of such multivariate
19 associations can be compromised by low statistical power and confounding by popula-
20 tion structure. Linear mixed effects models (LMM) can account for correlations due to
21 relatedness but have not been applicable in high-dimensional (HD) settings where the
22 number of fixed effect predictors greatly exceeds the number of samples. False positives
23 or false negatives can result from two-stage approaches, where the residuals estimated
24 from a null model adjusted for the subjects' relationship structure are subsequently
25 used as the response in a standard penalized regression model. To overcome these
26 challenges, we develop a general penalized LMM with a single random effect called
27 `gmmix` for simultaneous SNP selection and adjustment for population structure in high
28 dimensional prediction models. We develop a blockwise coordinate descent algorithm
29 with automatic tuning parameter selection which is highly scalable, computationally
30 efficient and has theoretical guarantees of convergence. Through simulations and three
31 real data examples, we show that `gmmix` leads to more parsimonious models compared
32 to the two-stage approach or principal component adjustment with better prediction
33 accuracy. Our method performs well even in the presence of highly correlated mark-
34 ers, and when the causal SNPs are included in the kinship matrix. `gmmix` can be used
35 to construct polygenic risk scores and select instrumental variables in Mendelian ran-
36 domization studies. Our algorithms are available in an R package available on CRAN
37 (<https://cran.r-project.org/package=gmmix>).

38 1 Author Summary

39 This work addresses a recurring challenge in the analysis and interpretation of genetic as-
40 sociation studies: which genetic variants can best predict and are independently associated
41 with a given phenotype in the presence of population structure ? Not controlling confound-
42 ing due to geographic population structure, family and/or cryptic relatedness can lead to
43 spurious associations. Much of the existing research has therefore focused on modeling the
44 association between a phenotype and a single genetic variant in a linear mixed model with

45 a random effect. However, this univariate approach may miss true associations due to the
46 stringent significance thresholds required to reduce the number of false positives and also
47 ignores the correlations between markers. We propose an alternative method for fitting
48 high-dimensional multivariable models, which selects SNPs that are independently associ-
49 ated with the phenotype while also accounting for population structure. We provide an
50 efficient implementation of our algorithm and show through simulation studies and real data
51 examples that our method outperforms existing methods in terms of prediction accuracy and
52 controlling the false discovery rate.

53 2 Introduction

54 Genome-wide association studies (GWAS) have become the standard method for analyzing
55 genetic datasets owing to their success in identifying thousands of genetic variants associated
56 with complex diseases (<https://www.genome.gov/gwastudies/>). Despite these impressive
57 findings, the discovered markers have only been able to explain a small proportion of the
58 phenotypic variance; this is known as the missing heritability problem [1]. One plausible
59 reason is that there are many causal variants that each explain a small amount of variation
60 with small effect sizes [2]. Methods such GWAS, which test each variant or single nucleotide
61 polymorphism (SNP) independently, may miss these true associations due to the stringent
62 significance thresholds required to reduce the number of false positives [1]. Another major
63 issue to overcome is that of confounding due to geographic population structure, family
64 and/or cryptic relatedness which can lead to spurious associations [3]. For example, there
65 may be subpopulations within a study that differ with respect to their genotype frequencies
66 at a particular locus due to geographical location or their ancestry. This heterogeneity in
67 genotype frequency can cause correlations with other loci and consequently mimic the signal
68 of association even though there is no biological association [4, 5]. Studies that separate
69 their sample by ethnicity to address this confounding suffer from a loss in statistical power

70 due to the drop in sample size.

71 To address the first problem, multivariable regression methods have been proposed which
72 simultaneously fit many SNPs in a single model [6, 7]. Indeed, the power to detect an
73 association for a given SNP may be increased when other causal SNPs have been accounted
74 for. Conversely, a stronger signal from a causal SNP may weaken false signals when modeled
75 jointly [6].

76 Solutions for confounding by population structure have also received significant attention in
77 the literature [8, 9, 10, 11]. There are two main approaches to account for the relatedness
78 between subjects: 1) the principal component (PC) adjustment method and 2) the linear
79 mixed model (LMM). The PC adjustment method includes the top PCs of genome-wide
80 SNP genotypes as additional covariates in the model [12]. The LMM uses an estimated
81 covariance matrix from the individuals' genotypes and includes this information in the form
82 of a random effect [3].

83 While these problems have been addressed in isolation, there has been relatively little
84 progress towards addressing them jointly at a large scale. Region-based tests of association
85 have been developed where a linear combination of p variants is regressed on the response
86 variable in a mixed model framework [13]. In case-control data, a stepwise logistic-regression
87 procedure was used to evaluate the relative importance of variants within a small genetic
88 region [14]. These methods however are not applicable in the high-dimensional setting, i.e.,
89 when the number of variables p is much larger than the sample size n , as is often the case in
90 genetic studies where millions of variants are measured on thousands of individuals.

91 There has been recent interest in using penalized linear mixed models, which place a con-
92 straint on the magnitude of the effect sizes while controlling for confounding factors such as
93 population structure. For example, the LMM-lasso [15] places a Laplace prior on all main
94 effects while the adaptive mixed lasso [16] uses the L_1 penalty [17] with adaptively chosen
95 weights [18] to allow for differential shrinkage amongst the variables in the model. Another

method applied a combination of both the lasso and group lasso penalties in order to select variants within a gene most associated with the response [19]. However, methods such as the LMM-lasso are normally performed in two steps. First, the variance components are estimated once from a LMM with a single random effect. These LMMs normally use the estimated covariance matrix from the individuals' genotypes to account for the relatedness but assumes no SNP main effects (i.e. a null model). The residuals from this null model with a single random effect can be treated as independent observations because the relatedness has been effectively removed from the original response. In the second step, these residuals are used as the response in any high-dimensional model that assumes uncorrelated errors. This approach has both computational and practical advantages since existing penalized regression software such as `glmnet` [20] and `gglasso` [21], which assume independent observations, can be applied directly to the residuals. However, recent work has shown that there can be a loss in power if a causal variant is included in the calculation of the covariance matrix as its effect will have been removed in the first step [13, 22].

In this paper we develop a general penalized LMM framework called `ggmix` that simultaneously selects variables and estimates their effects, accounting for between-individual correlations. We develop a blockwise coordinate descent algorithm with automatic tuning parameter selection which is highly scalable, computationally efficient and has theoretical guarantees of convergence. Our method can handle several sparsity inducing penalties such as the lasso [17] and elastic net [23]. Through simulations and three real data examples, we show that `ggmix` leads to more parsimonious models compared to the two-stage approach or principal component adjustment with better prediction accuracy. Our method performs well even in the presence of highly correlated markers, and when the causal SNPs are included in the kinship matrix. All of our algorithms are implemented in the `ggmix` R package hosted on CRAN with extensive documentation (<https://sahirbhatnagar.com/ggmix>). We provide a brief demonstration of the `ggmix` package in Appendix C.

122 The rest of the paper is organized as follows. In Section 3, we compare the performance
123 of our proposed approach and demonstrate the scenarios where it can be advantageous to
124 use over existing methods through simulation studies and three real data analyses. This is
125 followed by a discussion of our results, some limitations and future directions in Section 4.
126 Section 5 describes the `gmmix` model, the optimization procedure and the algorithm used to
127 fit it.

128 3 Results

129 In this section we demonstrate the performance of `gmmix` in a simulation study and three
130 real data applications.

131 3.1 Simulation Study

132 We evaluated the performance of `gmmix` in a variety of simulated scenarios. For each simula-
133 tion scenario we compared `gmmix` to the `lasso` and the `twostep` method. For the `lasso`, we
134 included the top 10 principal components from the simulated genotypes used to calculate the
135 kinship matrix as unpenalized predictors in the design matrix. For the `twostep` method, we
136 first fitted an intercept only model with a single random effect using the average information
137 restricted maximum likelihood (AIREML) algorithm [24] as implemented in the `gaston` R
138 package [25]. The residuals from this model were then used as the response in a regular
139 `lasso` model. Note that in the `twostep` method, we removed the kinship effect in the first
140 step and therefore did not need to make any further adjustments when fitting the penalized
141 model. We fitted the `lasso` using the default settings and `standardize=FALSE` in the `glmnet`
142 package [20], with 10-fold cross-validation (CV) to select the optimal tuning parameter. For
143 other parameters in our simulation study, we defined the following quantities:

- 144
 - n : sample size
 - c : percentage of causal SNPs

- 146 • β : true effect size vector of length p
- 147 • $S_0 = \{j; (\beta)_j \neq 0\}$ the index of the true active set with cardinality $|S_0| = c \times p$
- 148 • *causal*: the list of causal SNP indices
- 149 • *kinship*: the list of SNP indices for the kinship matrix
- 150 • \mathbf{X} : $n \times p$ matrix of SNPs that were included as covariates in the model

151 We simulated data from the model

$$\mathbf{Y} = \mathbf{X}\beta + \mathbf{P} + \boldsymbol{\varepsilon} \quad (1)$$

152 where $\mathbf{P} \sim \mathcal{N}(0, \eta\sigma^2\Phi)$ is the polygenic effect and $\boldsymbol{\varepsilon} \sim \mathcal{N}(0, (1 - \eta)\sigma^2\mathbf{I})$ is the error term.
 153 Here, $\Phi_{n \times n}$ is the covariance matrix based on the *kinship* SNPs from n individuals, $\mathbf{I}_{n \times n}$ is
 154 the identity matrix and parameters σ^2 and $\eta \in [0, 1]$ determine how the variance is divided
 155 between \mathbf{P} and $\boldsymbol{\varepsilon}$. The values of the parameters that we used were as follows: narrow
 156 sense heritability $\eta = \{0.1, 0.3\}$, number of covariates $p = 5,000$, number of *kinship* SNPs
 157 $k = 10,000$, percentage of *causal* SNPs $c = \{0\%, 1\%\}$ and $\sigma^2 = 1$. In addition to these
 158 parameters, we also varied the amount of overlap between the *causal* list and the *kinship*
 159 list. We considered two main scenarios:

- 160 1. None of the *causal* SNPs are included in *kinship* set.
- 161 2. All of the *causal* SNPs are included in the *kinship* set.

162 Both kinship matrices were meant to contrast the model behavior when the causal SNPs are
 163 included in both the main effects and random effects (referred to as proximal contamina-
 164 tion [8]) versus when the causal SNPs are only included in the main effects. These scenarios
 165 are motivated by the current standard of practice in GWAS where the candidate marker
 166 is excluded from the calculation of the kinship matrix [8]. This approach becomes much
 167 more difficult to apply in large-scale multivariable models where there is likely to be overlap

168 between the variables in the design matrix and kinship matrix. We simulated random geno-
 169 types from the BN-PSD admixture model with 1D geography and 10 subpopulations using
 170 the `bnpsd` package [26, 27]. In Figure 1, we plot the estimated kinship matrix from a single
 171 simulated dataset in the form of a heatmap where a darker color indicates a closer genetic
 172 relationship.

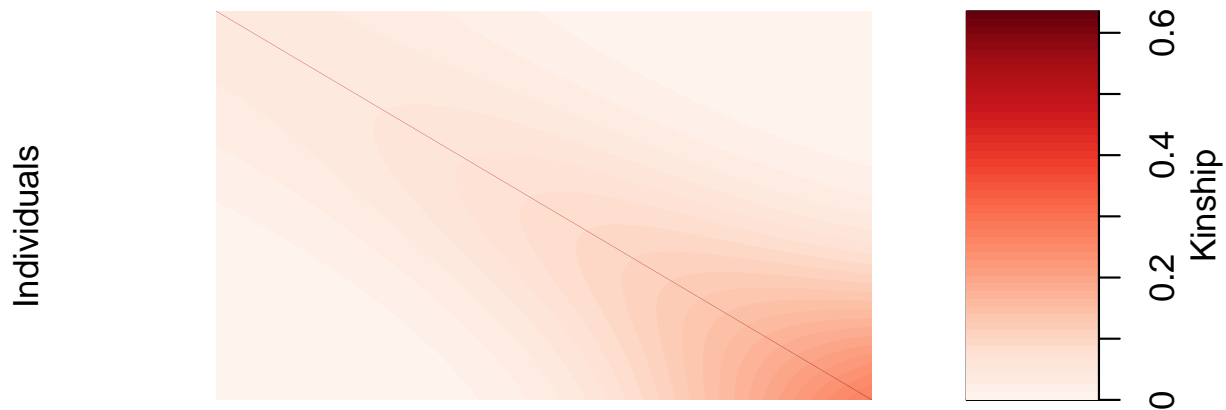


Figure 1: Example of an empirical kinship matrix used in simulation studies. This scenario models a 1D geography with extensive admixture.

173 In Figure 2 we plot the first two principal component scores calculated from the simulated
 174 genotypes used to calculate the kinship matrix in Figure 1, and color each point by sub-
 175 population membership. We can see that the PCs can identify the subpopulations which
 176 is why including them as additional covariates in a regression model has been considered a
 177 reasonable approach to control for confounding.

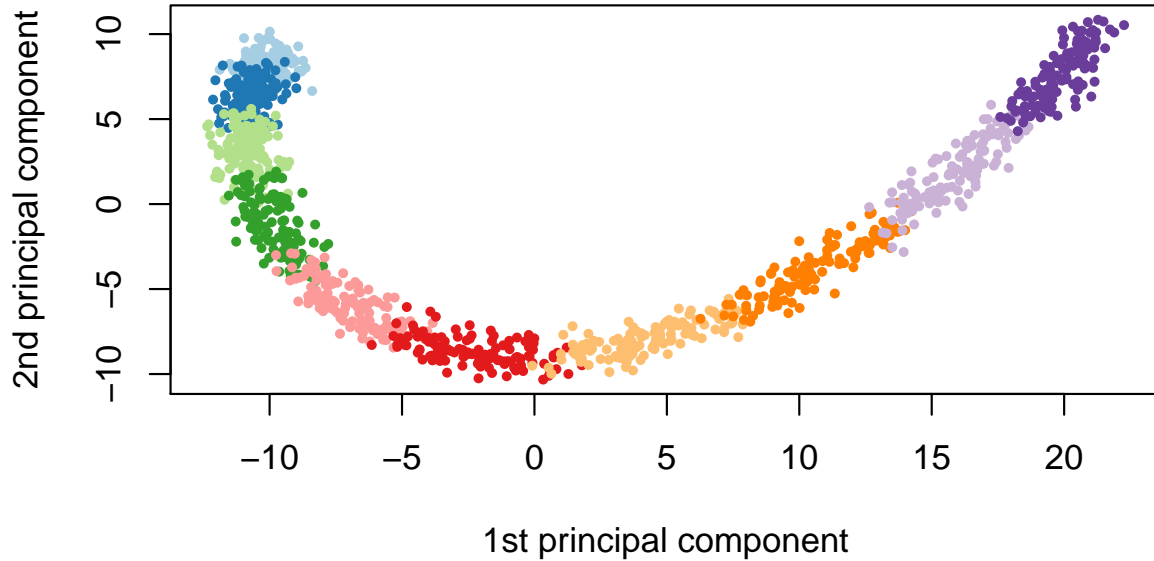


Figure 2: First two principal component scores of the genotype data used to estimate the kinship matrix where each color represents one of the 10 simulated subpopulations.

178 Using this set-up, we randomly partitioned 1000 simulated observations into 80% for training
 179 and 20% for testing. The training set was used to fit the model and select the optimal tuning
 180 parameter only, and the resulting model was evaluated on the test set. Let $\hat{\lambda}$ be the esti-
 181 mated value of the optimal regularization parameter, $\hat{\beta}_{\hat{\lambda}}$ the estimate of β at regulariza-
 182 tion parameter $\hat{\lambda}$, and $\hat{S}_{\hat{\lambda}} = \{j; (\hat{\beta}_{\hat{\lambda}})_j \neq 0\}$ the index of the set of non-zero estimated coefficients.
 183 To compare the methods in the context of true positive rate (TPR), we selected the largest
 184 tuning parameter that would result in a false positive rate (FPR) closest to 5%, but not
 185 more. Note that in practice, this approach to selecting the tuning parameter is generally
 186 not possible since we do not know the underlying true model in advance. For real data, we
 187 suggest an information criterion approach described in Section 5.3.8 or a sample splitting
 188 approach such as the one we used for the UK Biobank analysis shown in Section 3.2.1. We
 189 also compared the model size ($|\hat{S}_{\hat{\lambda}}|$), test set prediction error based on the refitted unpenal-

190 ized estimates for each selected model, the estimation error ($\|\hat{\beta} - \beta\|_2^2$), and the variance
191 components (η, σ^2) for the polygenic random effect and error term.

192 The results are summarized in Table 1. We see that `gmmix` outperformed the `twostep` in
193 terms of TPR, and was comparable to the `lasso`. This was the case, regardless of true heri-
194 tability and whether the causal SNPs were included in the calculation of the kinship matrix.

195 For the `twostep` however, the TPR at a FPR of 5%, drops, on average, from 0.84 (when
196 causal SNPs are not in the kinship) to 0.76 (when causal SNPs are in the kinship). Across
197 all simulation scenarios, `gmmix` had the smallest estimation error, and smallest root mean
198 squared prediction error (RMSE) on the test set while also producing the most parsimonious
199 models. Both the `lasso` and `twostep` selected more false positives, even in the null model
200 scenario. Both the `twostep` and `gmmix` overestimated the heritability though `gmmix` was
201 closer to the true value. When none of the causal SNPs were in the kinship, both methods
202 tended to overestimate the truth when $\eta = 10\%$ and underestimate when $\eta = 30\%$. Across
203 all simulation scenarios `gmmix` was able to (on average) correctly estimate the error variance.
204 The `lasso` tended to overestimate σ^2 in the null model while the `twostep` overestimated σ^2
205 when none of the causal SNPs were in the kinship matrix.

206 Overall, we observed that variable selection results and RMSE for `gmmix` were similar regard-
207 less of whether the causal SNPs were in the kinship matrix or not. This result is encouraging
208 since in practice the kinship matrix is constructed from a random sample of SNPs across the
209 genome, some of which are likely to be causal, particularly in polygenic traits.

210 In particular, our simulation results show that the principal component adjustment method
211 may not be the best approach to control for confounding by population structure, particularly
212 when variable selection is of interest.

Table 1: Mean (standard deviation) from 200 simulations stratified by the number of causal SNPs (null, 1%), the overlap between causal SNPs and kinship matrix (no overlap, all causal SNPs in kinship), and true heritability (10%, 30%). For all simulations, sample size is $n = 1000$, the number of covariates is $p = 5000$, and the number of SNPs used to estimate the kinship matrix is $k = 10000$. TPR at FPR=5% is the true positive rate at a fixed false positive rate of 5%. Model Size ($|\widehat{S}_{\lambda}|$) is the number of selected variables in the training set using the high-dimensional BIC for `gmmix` and 10-fold cross validation for `lasso` and `twostep`. RMSE is the root mean squared error on the test set. Estimation error is the squared distance between the estimated and true effect sizes. Error variance (σ^2) for `twostep` is estimated from an intercept only LMM with a single random effect and is modeled explicitly in `gmmix`. For the `lasso` we use $\frac{1}{n-|\widehat{S}_{\lambda}|} \|\mathbf{Y} - \mathbf{X}\widehat{\boldsymbol{\beta}}_{\lambda}\|_2^2$ [28] as an estimator for σ^2 . Heritability (η) for `twostep` is estimated as $\sigma_g^2 / (\sigma_g^2 + \sigma_e^2)$ from an intercept only LMM with a single random effect where σ_g^2 and σ_e^2 are the variance components for the random effect and error term, respectively. η is explicitly modeled in `gmmix`. There is no positive way to calculate η for the `lasso` since we are using a PC adjustment.

Metric	Method	Null model				1% Causal SNPs			
		No overlap		All causal SNPs in kinship		No overlap		All causal SNPs in kinship	
		10%	30%	10%	30%	10%	30%	10%	30%
TPR at FPR=5%	twostep	0.00 (0.00)	0.00 (0.00)	0.00 (0.00)	0.00 (0.00)	0.84 (0.05)	0.84 (0.05)	0.76 (0.09)	0.77 (0.08)
	lasso	0.00 (0.00)	0.00 (0.00)	0.00 (0.00)	0.00 (0.00)	0.86 (0.05)	0.85 (0.05)	0.86 (0.05)	0.86 (0.05)
	gmmix	0.00 (0.00)	0.00 (0.00)	0.00 (0.00)	0.00 (0.00)	0.86 (0.05)	0.86 (0.05)	0.85 (0.05)	0.86 (0.05)
	twostep	0 (0, 5) (289)	0 (0, 2) (287)	0 (0, 5) (388)	0 (0, 2) (385)	328 (250)	332 (329)	284 (319)	284 (253)
	lasso	0 (0, 6) (246)	0 (0, 5) (317)	0 (0, 6) (314)	0 (0, 5) (245)	278 (252)	276 (321)	279 (244)	285 (319)
	gmmix	0 (0, 0) (43)	0 (0, 0) (43)	0 (0, 0) (39)	0 (0, 0) (48)	43 (39, 49) (43)	43 (39, 48) (44)	44 (38, 49) (43)	43 (38, 48) (43)
	twostep	1.02 (0.07)	1.02 (0.06)	1.02 (0.07)	1.02 (0.06)	1.42 (0.10)	1.41 (0.10)	1.44 (0.33)	1.40 (0.22)
	lasso	1.02 (0.06)	1.02 (0.06)	1.02 (0.06)	1.02 (0.06)	1.39 (0.09)	1.38 (0.09)	1.40 (0.08)	1.38 (0.08)
	gmmix	1.00 (0.05)	1.00 (0.05)	1.00 (0.05)	1.00 (0.05)	1.22 (0.10)	1.20 (0.10)	1.23 (0.11)	1.23 (0.12)
Model Size	twostep	0.12 (0.22)	0.09 (0.19)	0.12 (0.22)	0.09 (0.19)	2.97 (0.60)	2.92 (0.60)	3.60 (5.41)	3.21 (3.46)
	lasso	0.13 (0.21)	0.12 (0.22)	0.13 (0.21)	0.12 (0.22)	2.76 (0.46)	2.69 (0.47)	2.82 (0.48)	2.75 (0.48)
	gmmix	0.00 (0.01)	0.01 (0.02)	0.00 (0.01)	0.01 (0.02)	2.11 (1.28)	2.04 (1.22)	2.21 (1.24)	2.28 (1.34)
	twostep	0.87 (0.11)	0.69 (0.15)	0.87 (0.11)	0.69 (0.15)	14.23 (3.53)	14.13 (3.52)	1.42 (1.71)	1.28 (1.66)
	lasso	0.98 (0.05)	0.96 (0.05)	0.98 (0.05)	0.96 (0.05)	1.04 (0.13)	1.02 (0.13)	1.03 (0.14)	1.01 (0.14)
Error Variance	gmmix	0.85 (0.18)	0.64 (0.20)	0.85 (0.18)	0.64 (0.20)	2.00 (0.49)	1.86 (0.51)	1.06 (0.46)	0.83 (0.45)
	twostep	0.13 (0.11)	0.31 (0.15)	0.13 (0.11)	0.31 (0.15)	0.26 (0.14)	0.26 (0.14)	0.92 (0.08)	0.93 (0.08)
	lasso	—	—	—	—	—	—	—	—
	gmmix	0.15 (0.18)	0.37 (0.21)	0.15 (0.18)	0.37 (0.21)	0.18 (0.16)	0.23 (0.17)	0.59 (0.20)	0.68 (0.19)

Note:

Median (Inter-quartile range) is given for Model Size.

213 **3.2 Real Data Applications**

214 Three datasets with different features were used to illustrate the potential advantages of
215 `gmmix` over existing approaches such as PC adjustment in a `lasso` regression. In the first
216 two datasets, family structure induced low levels of correlation and sparsity in signals. In
217 the last, a dataset involving mouse crosses, correlations were extremely strong and could
218 confound signals.

219 **3.2.1 UK Biobank**

220 With more than 500,000 participants, the UK Biobank is one of the largest genotyped health
221 care registries in the world. Among these participants, 147,731 have been inferred to be
222 related to at least one individual in this cohort [29]. Such a widespread genetic relatedness
223 may confound association studies and bias trait predictions if not properly accounted for.
224 Among these related individuals, 18,150 have a documented familial relationship (parent-
225 offspring, full siblings, second degree or third degree) that was previously inferred in [30]. We
226 attempted to derive a polygenic risk score for height among these individuals. As suggested
227 by a reviewer, the goal of this analysis was to see how the different methods performed for
228 a highly polygenic trait in a set of related individuals. We compared the `gmmix`-derived
229 polygenic risk score to those derived by the `twostep` and `lasso` methods.

230 We first estimated the pairwise kinship coefficient among the 18,150 reportedly related indi-
231 viduals based on 784,256 genotyped SNPs using KING [31]. We grouped related individuals
232 with a kinship coefficient > 0.044 [31] into 8,300 pedigrees. We then randomly split the
233 dataset into a training set, a model selection set and a test set of roughly equal sample size,
234 ensuring all individuals in the same pedigree were assigned into the same set. We inverse
235 normalized the standing height after adjusting for age, sex, genotyping array, and assessment
236 center following Yengo et al. [32].

237 To reduce computational complexity, we selected 10,000 SNPs with the largest effect sizes

associated with height from a recent large meta-analysis [32]. Among these 10,000 SNPs, 1,233 were genotyped and used for estimating the kinship whereas the other 8,767 SNPs were imputed based on the Haplotype Reference Consortium reference panel [33]. The distribution of the 10,000 SNPs by chromosome and whether or not the SNP was imputed is shown in Figure B.1 in Supplemental Section B. We see that every chromosome contributed SNPs to the model with 15% coming from chromosome 6. The markers we used are theoretically independent since Yengo et al. performed a COJO analysis which should have tuned down signals due to linkage disequilibrium [32]. We used `gmmix`, `twostep` and `lasso` to select SNPs most predictive of the inverse normalized height on the training set, and chose the λ with the lowest prediction RMSE on the model selection set for each method. We then examined the performance of each derived polygenic risk score on the test set. Similar to Section 3.1, we adjusted for the top 10 genetic PCs as unpenalized predictors when fitting the `lasso` models, and supplied the kinship matrix based on 784,256 genotyped SNPs to `gmmix` and `twostep`.

We found that with a kinship matrix estimated using all genotyped SNPs, `gmmix` had the possibility to achieve a lower RMSE on the model selection set compared to the `twostep` and `lasso` methods (Figure 3A). An optimized `gmmix`-derived polygenic risk score that utilized the least number of SNPs was also able to better predict the trait with lower RMSE on the test set (Figure 3B).

We additionally applied a Bayesian Sparse Linear Mixed Model (BSLMM) [34] implemented in the GEMMA package [35] to derive a polygenic risk score on the training set. A posterior probability of inclusion of each SNP was provided and prediction was based on all SNPs with a positive posterior probability. We found that although the BSLMM-based polygenic risk score leveraged the most SNPs, it did not achieve a comparable prediction accuracy as the other three methods (Figure 3B). Likely due to the small effect sizes of these SNPs, only 94, 35 and 1 SNPs had a posterior inclusion probability above 0.05, 0.10 and 0.50,

264 respectively. The model would have further reduced prediction accuracy if the prediction
 265 was based only on these SNPs.

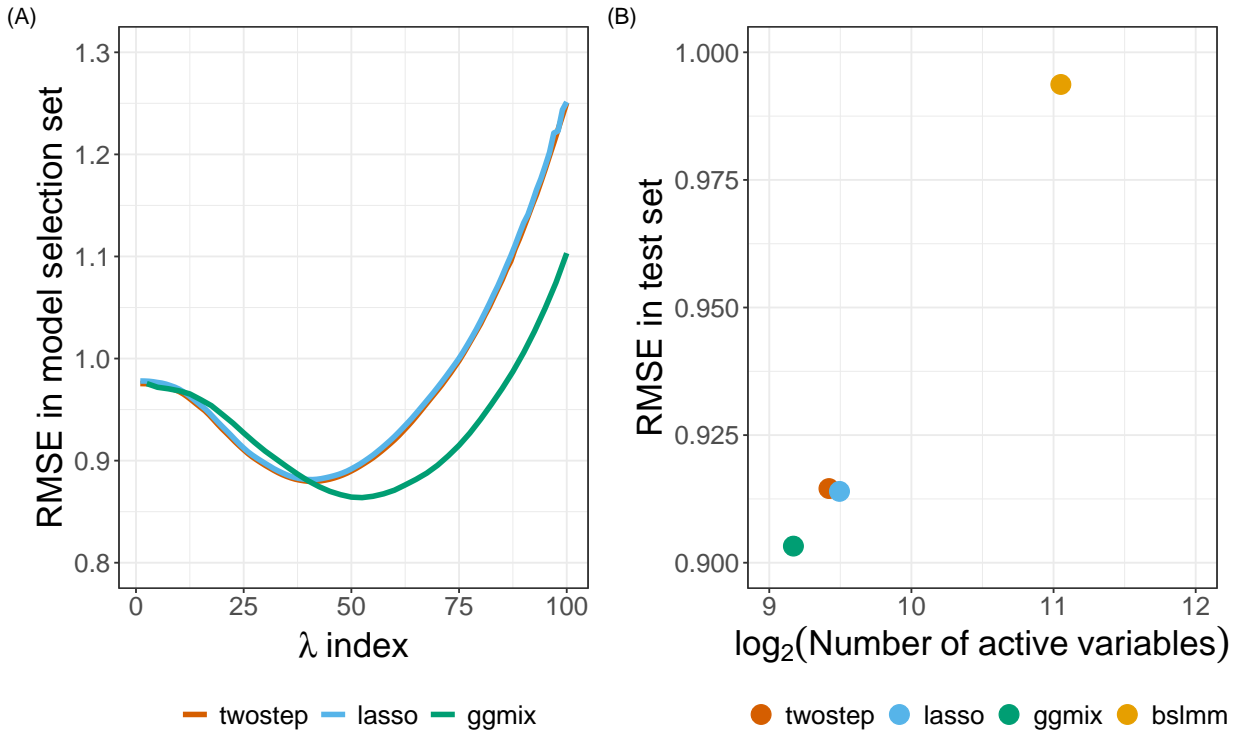


Figure 3: Model selection and testing in the UK Biobank. (A) Root-mean-square error of three methods on the model selection set with respect to a grid search of penalty factor used on the training set. (B) Performance of four methods on the test set with penalty factor optimized on the model selection set. The x-axis has a logarithmic scale. The BSLMM method optimized coefficients of each SNP through an MCMC process on the training set and was directly evaluated on the test set.

266 3.2.2 GAW20

267 In the most recent Genetic Analysis Workship 20 (GAW20), the causal modeling group in-
 268 vestigated causal relationships between DNA methylation (exposure) within some genes and
 269 the change in high-density lipoproteins Δ HDL (outcome) using Mendelian Randomization
 270 (MR) [36]. Penalized regression methods were used to select SNPs strongly associated with
 271 the exposure in order to be used as an instrumental variable (IV) [37, 38]. However, since
 272 GAW20 data consisted of families, **twostep** methods were used which could have resulted

273 in a large number of false positives or false negatives. `ggmix` now provides an alternative
274 approach that could be used for selecting the IV while accounting for the family structure
275 of the data.

276 We applied `ggmix` to all 200 GAW20 simulation datasets, each of 679 observations, and
277 compared its performance to the `twostep` and `lasso` methods. Using a Factored Spectrally
278 Transformed Linear Mixed Model (FaST-LMM) [39] adjusted for age and sex, we validated
279 the effect of rs9661059 on blood lipid trait to be significant (genome-wide $p = 6.29 \times 10^{-9}$).
280 Though several other SNPs were also associated with the phenotype, these associations were
281 probably mediated by CpG-SNP interaction pairs and did not reach statistical significance.
282 Therefore, to avoid ambiguity, we only focused on chromosome 1 containing 51,104 SNPs,
283 including rs9661059. Given that population admixture in the GAW20 data was likely, we
284 estimated the population kinship using REAP [40] after decomposing population composi-
285 tions using ADMIXTURE [41]. We used 100,276 LD-pruned whole-genome genotyped SNPs
286 for estimating the kinship. Among these, 8100 were included as covariates in our models
287 based on chromosome 1. The causal SNP was also among the 100,276 SNPs. All methods
288 were fit according to the same settings described in our simulation study in Section 3.1,
289 and adjusting for age and sex. We calculated the median (inter-quartile range) number of
290 active variables, and RMSE (standard deviation) based on five-fold CV on each simulated
291 dataset.

292 On each simulated replicate, we calibrated the methods so that they could be easily compared
293 by fixing the true positive rate to 1 and then minimizing the false positive rate. Hence, the
294 selected SNP, rs9661059, was likely to be the true positive for each method, and non-causal
295 SNPs were excluded to the greatest extent. All three methods precisely chose the correct
296 predictor without any false positives in more than half of the replicates, as the causal signal
297 was strong. However, when some false positives were selected (i.e. when the number of active
298 variables > 1), `ggmix` performed comparably to `twostep`, while the `lasso` was inclined to

299 select more false positives as suggested by the larger third quartile number of active variables
300 (Table 2). We also observed that `gmmix` outperformed the `twostep` method with lower CV
301 RMSE using the same number of SNPs. Meanwhile, it achieved roughly the same prediction
302 accuracy as `lasso` but with fewer non-causal SNPs (Table 2). It is also worth mentioning
303 that there was very little correlation between the causal SNP and SNPs within a 1Mb-
304 window around it (Figure B.2 in Supplemental Section B.2), making it an ideal scenario for
305 the `lasso` and related methods.

306 We also applied the `BSLMM` method by performing five-fold CV on each of the 200 simulated
307 replicates. We found that while `BSLMM` achieved a lower CV RMSE compared to the other
308 methods (Table 2), this higher prediction accuracy relied on approximately 80% of the 51,104
309 SNPs with a positive posterior inclusion probability. This may suggest overfitting in this
310 dataset. We additionally tried imposing a stricter posterior inclusion probability threshold
311 (0.05, 0.10 and 0.50) in order to improve feature selection. These thresholds however, resulted
312 in overly sparse models as most SNPs had a low posterior probability. It is also noteworthy
313 that we did not adjust for age and sex in the `BSLMM` model, as the current implementation
314 of the method in the `GEMMA` package does not allow adjustment for covariates.

Table 2: Summary of model performance based on 200 GAW20 simulations for the `twostep`, `lasso`, `gmmix` and `BSLMM` model with different posterior inclusion probability (PIP) thresholds. Five-fold cross-validation root-mean-square error (RMSE) was reported for each simulation replicate. Prediction performance was not reported for `BSLMM` with PIP greater than 0.05, 0.10 and 0.50 because some of the replications contained no active SNPs.

Method	Median number of active variables (Inter-quartile range)	RMSE (SD)
<code>twostep</code>	1 (1 - 11)	0.3604 (0.0242)
<code>lasso</code>	1 (1 - 15)	0.3105 (0.0199)
<code>gmmix</code>	1 (1 - 12)	0.3146 (0.0210)
<code>BSLMM</code> (PIP > 0)	40,737 (39,901 - 41,539)	0.2503 (0.0099)
<code>BSLMM</code> (PIP > 0.05)	2 (1 - 4)	
<code>BSLMM</code> (PIP > 0.10)	0 (0 - 1)	
<code>BSLMM</code> (PIP > 0.50)	0 (0 - 0)	

3.2.3 Mouse Crosses and Sensitivity to Mycobacterial Infection

Mouse inbred strains of genetically identical individuals are extensively used in research. Crosses of different inbred strains are useful for various studies of heritability focusing on either observable phenotypes or molecular mechanisms, and in particular, recombinant congenic strains have been an extremely useful resource for many years [42]. However, ignoring complex genetic relationships in association studies can lead to inflated false positives in genetic association studies when different inbred strains and their crosses are investigated [43, 44, 45]. Therefore, a previous study developed and implemented a mixed model to find loci associated with mouse sensitivity to mycobacterial infection [46]. The random effects in the model captured complex correlations between the recombinant congenic mouse strains based on the proportion of the DNA shared identical by descent. Through a series of mixed model fits at each marker, new loci that impact growth of mycobacteria on

328 chromosome 1 and chromosome 11 were identified.

329 Here we show that `gmmix` can identify these loci, as well as potentially others, in a single
330 analysis. We reanalyzed the growth permissiveness in the spleen, as measured by colony
331 forming units (CFUs), 6 weeks after infection from *Mycobacterium bovis* Bacille Calmette-
332 Guerin (BCG) Russia strain as reported in [46].

333 By taking the consensus between the “main model” and the “conditional model” of the original
334 study, we regarded markers D1Mit435 on chromosome 1 and D11Mit119 on chromosome 11
335 as two true positive loci. We directly estimated the kinship between mice using genotypes at
336 625 microsatellite markers. The estimated kinship entered directly into `gmmix` and `twostep`.

337 For the `lasso`, we calculated and included the first 10 principal components of the estimated
338 kinship. To evaluate the robustness of different models, we bootstrapped the 189-sample
339 dataset and repeated the analysis 200 times. We then conceived a two-fold criteria to evaluate
340 performance of each model. We first examined whether a model could pick up both true
341 positive loci using some λ . If the model failed to pick up both loci simultaneously with any
342 λ , we counted as modeling failure on the corresponding bootstrap replicate; otherwise, we
343 counted as modeling success and recorded which other loci were picked up given the largest
344 λ . Consequently, similar to the strategy used in the GAW20 analysis, we optimized the
345 models by tuning the penalty factor such that these two true positive loci were picked up,
346 while the number of other active loci was minimized. Significant markers were defined as
347 those captured in at least half of the successful bootstrap replicates (Figure 4).

348 We demonstrated that `gmmix` recognized the true associations more robustly than `twostep`
349 and `lasso`. In almost all (99%) bootstrap replicates, `gmmix` was able to capture both true
350 positives, while the `twostep` failed in 19% of the replicates and the `lasso` failed in 56% of
351 the replicates by missing at least one of the two true positives (Figure 4). The robustness
352 of `gmmix` is particularly noteworthy due to the strong correlations between all microsatellite
353 markers in this dataset (Figure B.3 in Supplemental Section B.2). These strong correlations

354 with the causal markers, partially explain the poor performance of the `lasso` as it suffers
355 from unstable selections in the presence of correlated variables (e.g. [47]).

356 We also identified several other loci that might also be associated with susceptibility to my-
357 cobacterial infection (Table 3). Among these new potentially-associated markers, D2Mit156
358 was found to play a role in control of parasite numbers of *Leishmania tropica* in lymph
359 nodes [48]. An earlier study identified a parent-of-origin effect at D17Mit221 on CD4M
360 levels [49]. This effect was more visible in crosses than in parental strains. In addition,
361 D14Mit131, selected only by `gmmix`, was found to have a 9% loss of heterozygosity in hy-
362 brids of two inbred mouse strains [50], indicating the potential presence of putative suppressor
363 genes pertaining to immune surveillance and tumor progression [51]. This result might also
364 suggest association with anti-bacterial responses yet to be discovered.

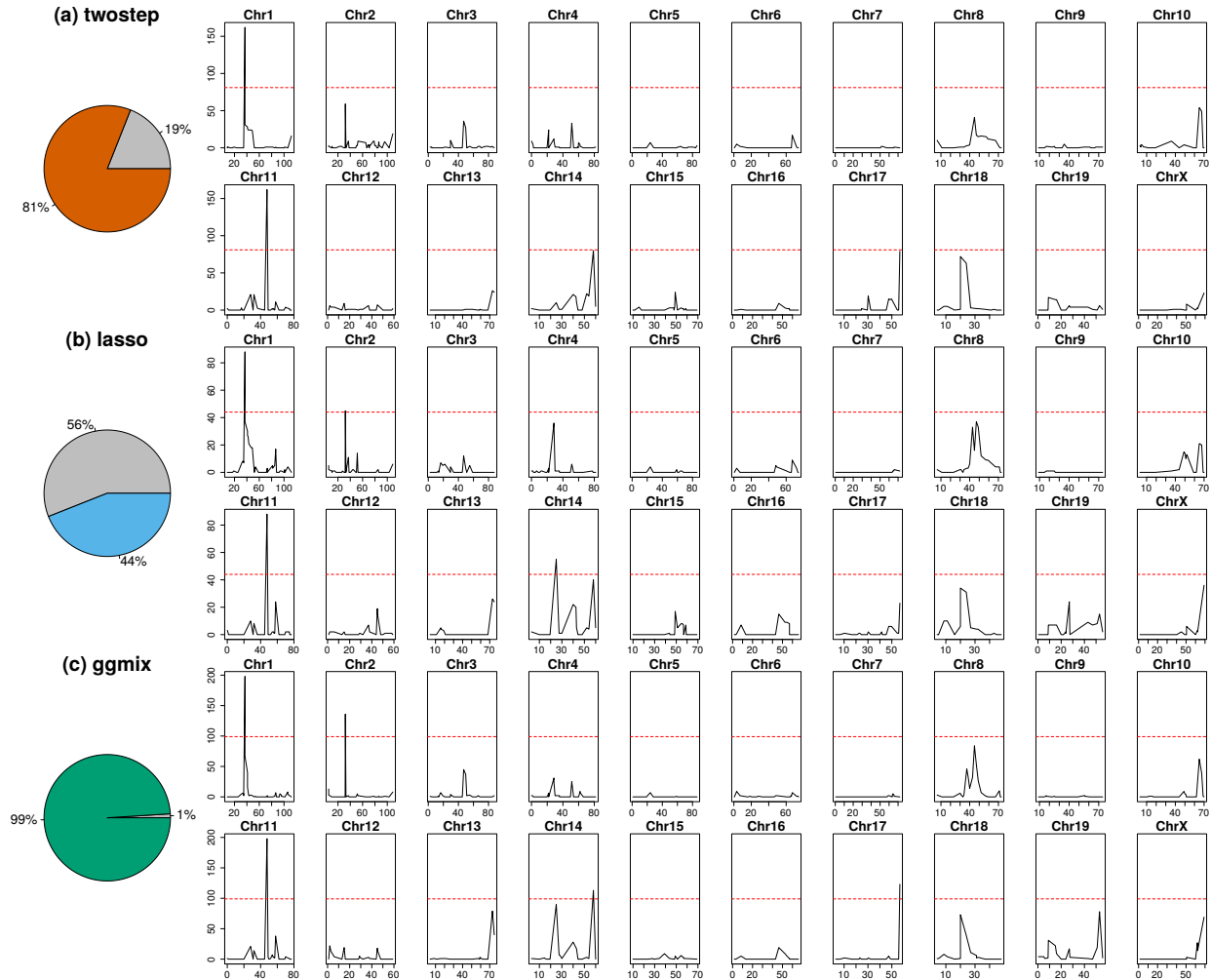


Figure 4: Comparison of model performance on the mouse cross data. Pie charts depict model robustness where grey areas denote bootstrap replicates on which the corresponding model is unable to capture both true positives using any penalty factor, whereas colored areas denote successful replicates. Chromosome-based signals record in how many successful replicates the corresponding loci are picked up by the corresponding optimized model. Red dashed lines delineate significance thresholds.

Table 3: Additional loci significantly associated with mouse susceptibility to myobacterial infection, after excluding two true positives. Loci needed to be identified in at least 50% of the successful bootstrap replicates that captured both true positive loci.

Method	Marker	Position in cM	Position in bp
twostep	N/A	N/A	N/A
³⁶⁵ lasso	D2Mit156	Chr2:31.66	Chr2:57081653-57081799
	D14Mit155	Chr14:31.52	Chr14:59828398-59828596
³⁶⁶ gmmix	D2Mit156	Chr2:31.66	Chr2:57081653-57081799
	D14Mit131	Chr14:63.59	Chr14:120006565-120006669
	D17Mit221	Chr17:59.77	Chr17:90087704-90087842

³⁶⁶ 4 Discussion

³⁶⁷ We have developed a general penalized LMM framework called **gmmix** which simultaneously
³⁶⁸ selects SNPs and adjusts for population structure in high dimensional prediction models. We
³⁶⁹ compared our method to the **twostage** procedure, where in the first stage, the dependence
³⁷⁰ between observations is adjusted for in a LMM with a single random effect and no covariates
³⁷¹ (i.e. null model). The residuals from this null model can then be used in any model for
³⁷² independent observations because the relatedness has been effectively removed from the
³⁷³ original response. We also compared our method to the **lasso** and **BSLMM** which are closely
³⁷⁴ related to **gmmix** since they also jointly model the relatedness and SNPs in a single step.
³⁷⁵ The key differences are that the **lasso** uses a principal component adjustment and **BSLMM** is
³⁷⁶ a Bayesian method focused on phenotype prediction.

³⁷⁷ Through an extensive simulation study and three real data analyses that mimic many ex-
³⁷⁸ perimental designs in genetics, we show that the current approaches of PC adjustment and
³⁷⁹ two-stage procedures are not necessarily sufficient to control for confounding by population
³⁸⁰ structure leading to a high number of false positives. Our simulation results show that **gmmix**

381 outperforms existing methods in terms of sparsity and prediction error even when the causal
382 variants are included in the kinship matrix (Table 1). Many methods for single-SNP analyses
383 avoid this proximal contamination [8] by using a leave-one-chromosome-out scheme [52], i.e.,
384 construct the kinship matrix using all chromosomes except the one on which the marker
385 being tested is located. However, this approach is not possible if we want to model many
386 SNPs (across many chromosomes) jointly to create, for example, a polygenic risk score. For
387 the purposes of variable selection, we would also want to model all chromosomes together
388 since the power to detect an association for a given SNP may be increased when other causal
389 SNPs have been accounted for. Conversely, a stronger signal from a causal SNP may weaken
390 false signals when modeled jointly [6], particularly when the markers are highly correlated
391 as in the mouse crosses example.

392 In the UK Biobank, we found that with a kinship matrix estimated using all genotyped SNPs,
393 `gmmix` had achieved a lower RMSE on the model selection set compared to the `twostep` and
394 `lasso` methods. Furthermore, an optimized `gmmix`-derived polygenic risk score that utilized
395 the least number of SNPs was also able to better predict the trait with lower RMSE on
396 the test set. In the GAW20 example, we showed that while all methods were able to select
397 the strongest causal SNP, `gmmix` did so with the least amount of false positives while also
398 maintaining good predictive ability. In the mouse crosses example, we showed that `gmmix` is
399 robust to perturbations in the data using a bootstrap analysis. Indeed, `gmmix` was able to
400 consistently select the true positives across bootstrap replicates, while `twostep` failed in 19%
401 of the replicates and `lasso` failed in 56% of the replicates by missing of at least one of the
402 two true positives. Our re-analysis of the data also lead to some potentially new findings, not
403 found by existing methods, that may warrant further study. This particular example had
404 many markers that were strongly correlated with each other (Figure B.3 of Supplemental
405 Section B.2). Nevertheless, we observed that the two true positive loci were the most often
406 selected while none of the nearby markers were picked up in more than 50% of the 200
407 bootstrap replicates. This shows that our method does recognize the true positives in the

408 presence of highly correlated markers. Nevertheless, we think the issue of variable selection
409 for correlated SNPs warrants further study. The recently proposed Precision Lasso [47] seeks
410 to address this problem in the high-dimensional fixed effects model.

411 We emphasize here that previously developed methods such as the LMM-lasso [15] use a two-
412 stage fitting procedure without any convergence details. From a practical point of view, there
413 is currently no implementation that provides a principled way of determining the sequence
414 of tuning parameters to fit, nor a procedure that automatically selects the optimal value of
415 the tuning parameter. To our knowledge, we are the first to develop a coordinate gradient
416 descent (CGD) algorithm in the specific context of fitting a penalized LMM for population
417 structure correction with theoretical guarantees of convergence. Furthermore, we develop
418 a principled method for automatic tuning parameter selection and provide an easy-to-use
419 software implementation in order to promote wider uptake of these more complex methods
420 by applied practitioners.

421 Although we derive a CGD algorithm for the ℓ_1 penalty, our approach can also be easily ex-
422 tended to other penalties such as the elastic net and group lasso with the same guarantees of
423 convergence. A limitation of `ggmix` is that it first requires computing the covariance matrix
424 with a computation time of $\mathcal{O}(n^2k)$ followed by a spectral decomposition of this matrix in
425 $\mathcal{O}(n^3)$ time where k is the number of SNP genotypes used to construct the covariance matrix.
426 This computation becomes prohibitive for large cohorts such as the UK Biobank [53] which
427 have collected genetic information on half a million individuals. When the matrix of geno-
428 types used to construct the covariance matrix is low rank, there are additional computational
429 speedups that can be implemented. While this has been developed for the univariate case [8],
430 to our knowledge, this has not been explored in the multivariable case. We are currently
431 developing a low rank version of the penalized LMM developed here, which reduces the time
432 complexity from $\mathcal{O}(n^2k)$ to $\mathcal{O}(nk^2)$. There is also the issue of how our model scales with
433 an increasing number of covariates (p). Due to the coordinate-wise optimization procedure,

434 we expect this to be less of an issue, but still prohibitive for $p > 1e5$. The `biglasso` pack-
435 age [54] uses memory mapping strategies for large p , and this is something we are exploring
436 for `gmmix`.

437 As was brought up by a reviewer, the simulations and real data analyses presented here
438 contained many more markers used to estimate the kinship than the sample size ($n/k \leq 0.1$).

439 In the single locus association test, Yang et al. [22] found that proximal contamination was
440 an issue when $n/k \approx 1$. We believe further theoretical study is needed to see if these results
441 can be generalized to the multivariable models being fit here. Once the computational
442 limitations of sample size mentioned above have been addressed, these theoretical results
443 can be supported by simulation studies.

444 There are other applications in which our method could be used as well. For example, there
445 has been a renewed interest in polygenic risk scores (PRS) which aim to predict complex
446 diseases from genotypes. `gmmix` could be used to build a PRS with the distinct advantage
447 of modeling SNPs jointly, allowing for main effects as well as interactions to be accounted
448 for. Based on our results, `gmmix` has the potential to produce more robust and parsimonious
449 models than the `lasso` with better predictive accuracy. Our method is also suitable for fine
450 mapping SNP association signals in genomic regions, where the goal is to pinpoint individual
451 variants most likely to impact the underlying biological mechanisms of disease [55].

452

5 Materials and Methods

453

5.1 Model Set-up

454 Let $i = 1, \dots, N$ be a grouping index, $j = 1, \dots, n_i$ the observation index within a group
455 and $N_T = \sum_{i=1}^N n_i$ the total number of observations. For each group let $\mathbf{y}_i = (y_1, \dots, y_{n_i})$ be
456 the observed vector of responses or phenotypes, \mathbf{X}_i an $n_i \times (p + 1)$ design matrix (with
457 the column of 1s for the intercept), \mathbf{b}_i a group-specific random effect vector of length

458 n_i and $\boldsymbol{\varepsilon}_i = (\varepsilon_{i1}, \dots, \varepsilon_{in_i})$ the individual error terms. Denote the stacked vectors $\mathbf{Y} =$
459 $(\mathbf{y}_i, \dots, \mathbf{y}_N)^T \in \mathbb{R}^{N_T \times 1}$, $\mathbf{b} = (\mathbf{b}_i, \dots, \mathbf{b}_N)^T \in \mathbb{R}^{N_T \times 1}$, $\boldsymbol{\varepsilon} = (\boldsymbol{\varepsilon}_i, \dots, \boldsymbol{\varepsilon}_N)^T \in \mathbb{R}^{N_T \times 1}$, and the
460 stacked matrix

461 $\mathbf{X} = (\mathbf{X}_1^T, \dots, \mathbf{X}_N^T) \in \mathbb{R}^{N_T \times (p+1)}$. Furthermore, let $\boldsymbol{\beta} = (\beta_0, \beta_1, \dots, \beta_p)^T \in \mathbb{R}^{(p+1) \times 1}$ be a vec-
462 tor of fixed effects regression coefficients corresponding to \mathbf{X} . We consider the following
463 linear mixed model with a single random effect [56]:

$$\mathbf{Y} = \mathbf{X}\boldsymbol{\beta} + \mathbf{b} + \boldsymbol{\varepsilon} \quad (2)$$

464 where the random effect \mathbf{b} and the error variance $\boldsymbol{\varepsilon}$ are assigned the distributions

$$\mathbf{b} \sim \mathcal{N}(0, \eta\sigma^2\boldsymbol{\Phi}) \quad \boldsymbol{\varepsilon} \sim \mathcal{N}(0, (1 - \eta)\sigma^2\mathbf{I}) \quad (3)$$

465 Here, $\boldsymbol{\Phi}_{N_T \times N_T}$ is a known positive semi-definite and symmetric covariance or kinship ma-
466 trix calculated from SNPs sampled across the genome, $\mathbf{I}_{N_T \times N_T}$ is the identity matrix and
467 parameters σ^2 and $\eta \in [0, 1]$ determine how the variance is divided between \mathbf{b} and $\boldsymbol{\varepsilon}$. Note
468 that η is also the narrow-sense heritability (h^2), defined as the proportion of phenotypic
469 variance attributable to the additive genetic factors [1]. The joint density of \mathbf{Y} is therefore
470 multivariate normal:

$$\mathbf{Y}|(\boldsymbol{\beta}, \eta, \sigma^2) \sim \mathcal{N}(\mathbf{X}\boldsymbol{\beta}, \eta\sigma^2\boldsymbol{\Phi} + (1 - \eta)\sigma^2\mathbf{I}) \quad (4)$$

471 The LMM-Lasso method [15] considers an alternative but equivalent parameterization given
472 by:

$$\mathbf{Y}|(\boldsymbol{\beta}, \delta, \sigma_g^2) \sim \mathcal{N}(\mathbf{X}\boldsymbol{\beta}, \sigma_g^2(\boldsymbol{\Phi} + \delta\mathbf{I})) \quad (5)$$

where $\delta = \sigma_e^2/\sigma_g^2$, σ_g^2 is the genetic variance and σ_e^2 is the residual variance. We instead
consider the parameterization in (4) since maximization is easier over the compact set $\eta \in$

[0, 1] than over the unbounded interval $\delta \in [0, \infty)$ [56]. We define the complete parameter vector as $\Theta := (\beta, \eta, \sigma^2)$. The negative log-likelihood for (4) is given by

$$-\ell(\Theta) \propto \frac{N_T}{2} \log(\sigma^2) + \frac{1}{2} \log(\det(\mathbf{V})) + \frac{1}{2\sigma^2} (\mathbf{Y} - \mathbf{X}\beta)^T \mathbf{V}^{-1} (\mathbf{Y} - \mathbf{X}\beta) \quad (6)$$

⁴⁷³ where $\mathbf{V} = \eta\Phi + (1 - \eta)\mathbf{I}$ and $\det(\mathbf{V})$ is the determinant of \mathbf{V} .

Let $\Phi = \mathbf{U}\mathbf{D}\mathbf{U}^T$ be the eigen (spectral) decomposition of the kinship matrix Φ , where $\mathbf{U}_{N_T \times N_T}$ is an orthonormal matrix of eigenvectors (i.e. $\mathbf{U}\mathbf{U}^T = \mathbf{I}$) and $\mathbf{D}_{N_T \times N_T}$ is a diagonal matrix of eigenvalues Λ_i . \mathbf{V} can then be further simplified [56]

$$\begin{aligned} \mathbf{V} &= \eta\Phi + (1 - \eta)\mathbf{I} \\ &= \eta\mathbf{U}\mathbf{D}\mathbf{U}^T + (1 - \eta)\mathbf{U}\mathbf{I}\mathbf{U}^T \\ &= \mathbf{U}\eta\mathbf{D}\mathbf{U}^T + \mathbf{U}(1 - \eta)\mathbf{I}\mathbf{U}^T \\ &= \mathbf{U}(\eta\mathbf{D} + (1 - \eta)\mathbf{I})\mathbf{U}^T \\ &= \mathbf{U}\tilde{\mathbf{D}}\mathbf{U}^T \end{aligned} \quad (7)$$

where

$$\tilde{\mathbf{D}} = \eta \mathbf{D} + (1 - \eta) \mathbf{I} \quad (8)$$

$$\begin{aligned} &= \eta \begin{bmatrix} \Lambda_1 & & & \\ & \Lambda_2 & & \\ & & \ddots & \\ & & & \Lambda_{N_T} \end{bmatrix} + (1 - \eta) \begin{bmatrix} 1 & & & \\ & 1 & & \\ & & \ddots & \\ & & & 1 \end{bmatrix} \\ &= \begin{bmatrix} 1 + \eta(\Lambda_1 - 1) & & & \\ & 1 + \eta(\Lambda_2 - 1) & & \\ & & \ddots & \\ & & & 1 + \eta(\Lambda_{N_T} - 1) \end{bmatrix} \\ &= \text{diag}\{1 + \eta(\Lambda_1 - 1), 1 + \eta(\Lambda_2 - 1), \dots, 1 + \eta(\Lambda_{N_T} - 1)\} \end{aligned} \quad (9)$$

Since (8) is a diagonal matrix, its inverse is also a diagonal matrix:

$$\tilde{\mathbf{D}}^{-1} = \text{diag} \left\{ \frac{1}{1 + \eta(\Lambda_1 - 1)}, \frac{1}{1 + \eta(\Lambda_2 - 1)}, \dots, \frac{1}{1 + \eta(\Lambda_{N_T} - 1)} \right\} \quad (10)$$

From (7) and (9), $\log(\det(\mathbf{V}))$ simplifies to

$$\begin{aligned} \log(\det(\mathbf{V})) &= \log \left(\det(\mathbf{U}) \det(\tilde{\mathbf{D}}) \det(\mathbf{U}^T) \right) \\ &= \log \left\{ \prod_{i=1}^{N_T} (1 + \eta(\Lambda_i - 1)) \right\} \\ &= \sum_{i=1}^{N_T} \log(1 + \eta(\Lambda_i - 1)) \end{aligned} \quad (11)$$

since $\det(\mathbf{U}) = 1$. It also follows from (7) that

$$\begin{aligned}\mathbf{V}^{-1} &= \left(\mathbf{U} \tilde{\mathbf{D}} \mathbf{U}^T \right)^{-1} \\ &= (\mathbf{U}^T)^{-1} \left(\tilde{\mathbf{D}} \right)^{-1} \mathbf{U}^{-1} \\ &= \mathbf{U} \tilde{\mathbf{D}}^{-1} \mathbf{U}^T\end{aligned}\tag{12}$$

since for an orthonormal matrix $\mathbf{U}^{-1} = \mathbf{U}^T$. Substituting (10), (11) and (12) into (6) the negative log-likelihood becomes

$$\begin{aligned}-\ell(\boldsymbol{\Theta}) &\propto \frac{N_T}{2} \log(\sigma^2) + \frac{1}{2} \sum_{i=1}^{N_T} \log(1 + \eta(\Lambda_i - 1)) + \frac{1}{2\sigma^2} (\mathbf{Y} - \mathbf{X}\boldsymbol{\beta})^T \mathbf{U} \tilde{\mathbf{D}}^{-1} \mathbf{U}^T (\mathbf{Y} - \mathbf{X}\boldsymbol{\beta}) \\ &\quad (13)\end{aligned}$$

$$\begin{aligned}&= \frac{N_T}{2} \log(\sigma^2) + \frac{1}{2} \sum_{i=1}^{N_T} \log(1 + \eta(\Lambda_i - 1)) + \frac{1}{2\sigma^2} (\mathbf{U}^T \mathbf{Y} - \mathbf{U}^T \mathbf{X}\boldsymbol{\beta})^T \tilde{\mathbf{D}}^{-1} (\mathbf{U}^T \mathbf{Y} - \mathbf{U}^T \mathbf{X}\boldsymbol{\beta}) \\ &= \frac{N_T}{2} \log(\sigma^2) + \frac{1}{2} \sum_{i=1}^{N_T} \log(1 + \eta(\Lambda_i - 1)) + \frac{1}{2\sigma^2} (\tilde{\mathbf{Y}} - \tilde{\mathbf{X}}\boldsymbol{\beta})^T \tilde{\mathbf{D}}^{-1} (\tilde{\mathbf{Y}} - \tilde{\mathbf{X}}\boldsymbol{\beta}) \\ &= \frac{N_T}{2} \log(\sigma^2) + \frac{1}{2} \sum_{i=1}^{N_T} \log(1 + \eta(\Lambda_i - 1)) + \frac{1}{2\sigma^2} \sum_{i=1}^{N_T} \frac{\left(\tilde{Y}_i - \sum_{j=0}^p \tilde{X}_{ij+1} \beta_j \right)^2}{1 + \eta(\Lambda_i - 1)}\end{aligned}\tag{14}$$

474 where $\tilde{\mathbf{Y}} = \mathbf{U}^T \mathbf{Y}$, $\tilde{\mathbf{X}} = \mathbf{U}^T \mathbf{X}$, \tilde{Y}_i denotes the i^{th} element of $\tilde{\mathbf{Y}}$, \tilde{X}_{ij} is the i, j^{th} entry of $\tilde{\mathbf{X}}$

475 and $\mathbf{1}$ is a column vector of N_T ones.

476 5.2 Penalized Maximum Likelihood Estimator

477 We define the $p + 3$ length vector of parameters $\boldsymbol{\Theta} := (\Theta_0, \Theta_1, \dots, \Theta_{p+1}, \Theta_{p+2}, \Theta_{p+3}) =$
478 $(\boldsymbol{\beta}, \eta, \sigma^2)$ where $\boldsymbol{\beta} \in \mathbb{R}^{p+1}$, $\eta \in [0, 1]$, $\sigma^2 > 0$. In what follows, $p + 2$ and $p + 3$ are the indices
479 in $\boldsymbol{\Theta}$ for η and σ^2 , respectively. In light of our goals to select variables associated with the
480 response in high-dimensional data, we propose to place a constraint on the magnitude of
481 the regression coefficients. This can be achieved by adding a penalty term to the likelihood
482 function (14). The penalty term is a necessary constraint because in our applications, the

483 sample size is much smaller than the number of predictors. We define the following objective
484 function:

$$Q_\lambda(\Theta) = f(\Theta) + \lambda \sum_{j \neq 0} v_j P_j(\beta_j) \quad (15)$$

485 where $f(\Theta) := -\ell(\Theta)$ is defined in (14), $P_j(\cdot)$ is a penalty term on the fixed regression
486 coefficients $\beta_1, \dots, \beta_{p+1}$ (we do not penalize the intercept) controlled by the nonnegative
487 regularization parameter λ , and v_j is the penalty factor for j th covariate. These penalty
488 factors serve as a way of allowing parameters to be penalized differently. Note that we do
489 not penalize η or σ^2 . An estimate of the regression parameters $\widehat{\Theta}_\lambda$ is obtained by

$$\widehat{\Theta}_\lambda = \arg \min_{\Theta} Q_\lambda(\Theta) \quad (16)$$

490 This is the general set-up for our model. In Section 5.3 we provide more specific details on
491 how we solve (16). We note here that the main difference between the proposed model, and
492 the `lmmlasso` [57], is that we rotate the response vector Y and the design matrix X by the
493 eigen vectors of the kinship matrix. This results in a diagonal covariance matrix making our
494 method orders of magnitude faster and usable for high-dimensional genetic data. A secondary
495 difference is that we are limiting ourselves to a single unpenalized random effect.

496 5.3 Computational Algorithm

497 We use a general purpose block coordinate gradient descent algorithm (CGD) [58] to solve (16).
498 At each iteration, we cycle through the coordinates and minimize the objective function with
499 respect to one coordinate only. For continuously differentiable $f(\cdot)$ and convex and block-
500 separable $P(\cdot)$ (i.e. $P(\beta) = \sum_i P_i(\beta_i)$), Tseng and Yun [58] show that the solution generated
501 by the CGD method is a stationary point of $Q_\lambda(\cdot)$ if the coordinates are updated in a
502 Gauss-Seidel manner i.e. $Q_\lambda(\cdot)$ is minimized with respect to one parameter while holding
503 all others fixed. The CGD algorithm has been successfully applied in fixed effects models
504 (e.g. [59], [20]) and linear mixed models with an ℓ_1 penalty [57]. In the next section we

505 provide some brief details about Algorithm 1. A more thorough treatment of the algorithm
 506 is given in Appendix A.

Algorithm 1: Block Coordinate Gradient Descent

Set the iteration counter $k \leftarrow 0$, initial values for the parameter vector $\Theta^{(0)}$ and convergence threshold ϵ ;

for $\lambda \in \{\lambda_{\max}, \dots, \lambda_{\min}\}$ **do**

repeat

$$\boldsymbol{\beta}^{(k+1)} \leftarrow \arg \min_{\boldsymbol{\beta}} Q_\lambda \left(\boldsymbol{\beta}, \eta^{(k)}, \sigma^2^{(k)} \right)$$

$$\eta^{(k+1)} \leftarrow \arg \min_{\eta} Q_\lambda \left(\boldsymbol{\beta}^{(k+1)}, \eta, \sigma^2^{(k)} \right)$$

$$\sigma^2^{(k+1)} \leftarrow \arg \min_{\sigma^2} Q_\lambda \left(\boldsymbol{\beta}^{(k+1)}, \eta^{(k+1)}, \sigma^2 \right)$$

$$k \leftarrow k + 1$$

until convergence criterion is satisfied: $\|\Theta^{(k+1)} - \Theta^{(k)}\|_2 < \epsilon$;

end

507 **5.3.1 Updates for the β parameter**

508 Recall that the part of the objective function that depends on β has the form

$$Q_\lambda(\Theta) = \frac{1}{2} \sum_{i=1}^{N_T} w_i \left(\tilde{Y}_i - \sum_{j=0}^p \tilde{X}_{ij} \beta_j \right)^2 + \lambda \sum_{j=1}^p v_j |\beta_j| \quad (17)$$

509 where

$$w_i := \frac{1}{\sigma^2 (1 + \eta(\Lambda_i - 1))} \quad (18)$$

Conditional on $\eta^{(k)}$ and $\sigma^2^{(k)}$, it can be shown that the solution for β_j , $j = 1, \dots, p$ is given by

$$\beta_j^{(k+1)} \leftarrow \frac{\mathcal{S}_\lambda \left(\sum_{i=1}^{N_T} w_i \tilde{X}_{ij} \left(\tilde{Y}_i - \sum_{\ell \neq j} \tilde{X}_{i\ell} \beta_\ell^{(k)} \right) \right)}{\sum_{i=1}^{N_T} w_i \tilde{X}_{ij}^2} \quad (19)$$

where $\mathcal{S}_\lambda(x)$ is the soft-thresholding operator

$$\mathcal{S}_\lambda(x) = \text{sign}(x)(|x| - \lambda)_+$$

510 $\text{sign}(x)$ is the signum function

$$\text{sign}(x) = \begin{cases} -1 & x < 0 \\ 0 & x = 0 \\ 1 & x > 0 \end{cases}$$

511 and $(x)_+ = \max(x, 0)$. We provide the full derivation in Appendix A.1.2.

512 5.3.2 Updates for the η parameter

513 Given $\beta^{(k+1)}$ and $\sigma^{2(k)}$, solving for $\eta^{(k+1)}$ becomes a univariate optimization problem:

$$\eta^{(k+1)} \leftarrow \arg \min_{\eta} \frac{1}{2} \sum_{i=1}^{N_T} \log(1 + \eta(\Lambda_i - 1)) + \frac{1}{2\sigma^{2(k)}} \sum_{i=1}^{N_T} \frac{\left(\tilde{Y}_i - \sum_{j=0}^p \tilde{X}_{ij+1} \beta_j^{(k+1)}\right)^2}{1 + \eta(\Lambda_i - 1)} \quad (20)$$

514 We use a bound constrained optimization algorithm [60] implemented in the `optim` function

515 in R and set the lower and upper bounds to be 0.01 and 0.99, respectively.

516 5.3.3 Updates for the σ^2 parameter

517 Conditional on $\beta^{(k+1)}$ and $\eta^{(k+1)}$, $\sigma^{2(k+1)}$ can be solved for using the following equation:

$$\sigma^{2(k+1)} \leftarrow \arg \min_{\sigma^2} \frac{N_T}{2} \log(\sigma^2) + \frac{1}{2\sigma^2} \sum_{i=1}^{N_T} \frac{\left(\tilde{Y}_i - \sum_{j=0}^p \tilde{X}_{ij+1} \beta_j\right)^2}{1 + \eta(\Lambda_i - 1)} \quad (21)$$

There exists an analytic solution for (21) given by:

$$\sigma^2(k+1) \leftarrow \frac{1}{N_T} \sum_{i=1}^{N_T} \frac{\left(\tilde{Y}_i - \sum_{j=0}^p \tilde{X}_{ij+1} \beta_j^{(k+1)}\right)^2}{1 + \eta^{(k+1)}(\Lambda_i - 1)} \quad (22)$$

5.3.4 Regularization path

In this section we describe how determine the sequence of tuning parameters λ at which to fit the model. Recall that our objective function has the form

$$Q_\lambda(\Theta) = \frac{N_T}{2} \log(\sigma^2) + \frac{1}{2} \sum_{i=1}^{N_T} \log(1 + \eta(\Lambda_i - 1)) + \frac{1}{2} \sum_{i=1}^{N_T} w_i \left(\tilde{Y}_i - \sum_{j=0}^p \tilde{X}_{ij+1} \beta_j \right)^2 + \lambda \sum_{j=1}^p v_j |\beta_j| \quad (23)$$

The Karush-Kuhn-Tucker (KKT) optimality conditions for (23) are given by:

$$\begin{aligned} \frac{\partial}{\partial \beta_1, \dots, \beta_p} Q_\lambda(\Theta) &= \mathbf{0}_p \\ \frac{\partial}{\partial \beta_0} Q_\lambda(\Theta) &= 0 \\ \frac{\partial}{\partial \eta} Q_\lambda(\Theta) &= 0 \\ \frac{\partial}{\partial \sigma^2} Q_\lambda(\Theta) &= 0 \end{aligned} \quad (24)$$

522 The equations in (24) are equivalent to

$$\begin{aligned}
 & \sum_{i=1}^{N_T} w_i \tilde{X}_{i1} \left(\tilde{Y}_i - \sum_{j=0}^p \tilde{X}_{ij+1} \beta_j \right) = 0 \\
 & \frac{1}{v_j} \sum_{i=1}^{N_T} w_i \tilde{X}_{ij} \left(\tilde{Y}_i - \sum_{j=0}^p \tilde{X}_{ij+1} \beta_j \right) = \lambda \gamma_j, \\
 & \gamma_j \in \begin{cases} \text{sign}(\hat{\beta}_j) & \text{if } \hat{\beta}_j \neq 0 \\ [-1, 1] & \text{if } \hat{\beta}_j = 0 \end{cases}, \quad \text{for } j = 1, \dots, p \\
 & \frac{1}{2} \sum_{i=1}^{N_T} \frac{\Lambda_i - 1}{1 + \eta(\Lambda_i - 1)} \left(1 - \frac{\left(\tilde{Y}_i - \sum_{j=0}^p \tilde{X}_{ij+1} \beta_j \right)^2}{\sigma^2 (1 + \eta(\Lambda_i - 1))} \right) = 0 \\
 & \sigma^2 - \frac{1}{N_T} \sum_{i=1}^{N_T} \frac{\left(\tilde{Y}_i - \sum_{j=0}^p \tilde{X}_{ij+1} \beta_j \right)^2}{1 + \eta(\Lambda_i - 1)} = 0
 \end{aligned} \tag{25}$$

523 where w_i is given by (18), $\tilde{\mathbf{X}}_{-1}^T$ is $\tilde{\mathbf{X}}^T$ with the first column removed, $\tilde{\mathbf{X}}_1^T$ is the first column
 524 of $\tilde{\mathbf{X}}^T$, and $\gamma \in \mathbb{R}^p$ is the subgradient function of the ℓ_1 norm evaluated at $(\hat{\beta}_1, \dots, \hat{\beta}_p)$.

525 Therefore $\widehat{\Theta}$ is a solution in (16) if and only if $\widehat{\Theta}$ satisfies (25) for some γ . We can determine
 526 a decreasing sequence of tuning parameters by starting at a maximal value for $\lambda = \lambda_{max}$
 527 for which $\hat{\beta}_j = 0$ for $j = 1, \dots, p$. In this case, the KKT conditions in (25) are equivalent
 528 to

$$\begin{aligned}
 & \frac{1}{v_j} \sum_{i=1}^{N_T} \left| w_i \tilde{X}_{ij} \left(\tilde{Y}_i - \tilde{X}_{i1} \beta_0 \right) \right| \leq \lambda, \quad \forall j = 1, \dots, p \\
 & \beta_0 = \frac{\sum_{i=1}^{N_T} w_i \tilde{X}_{i1} \tilde{Y}_i}{\sum_{i=1}^{N_T} w_i \tilde{X}_{i1}^2} \\
 & \frac{1}{2} \sum_{i=1}^{N_T} \frac{\Lambda_i - 1}{1 + \eta(\Lambda_i - 1)} \left(1 - \frac{\left(\tilde{Y}_i - \tilde{X}_{i1} \beta_0 \right)^2}{\sigma^2 (1 + \eta(\Lambda_i - 1))} \right) = 0 \\
 & \sigma^2 = \frac{1}{N_T} \sum_{i=1}^{N_T} \frac{\left(\tilde{Y}_i - \tilde{X}_{i1} \beta_0 \right)^2}{1 + \eta(\Lambda_i - 1)}
 \end{aligned} \tag{26}$$

529 We can solve the KKT system of equations in (26) (with a numerical solution for η) in order

530 to have an explicit form of the stationary point $\widehat{\Theta}_0 = \left\{ \widehat{\beta}_0, \mathbf{0}_p, \widehat{\eta}, \widehat{\sigma}^2 \right\}$. Once we have $\widehat{\Theta}_0$, we
531 can solve for the smallest value of λ such that the entire vector $(\widehat{\beta}_1, \dots, \widehat{\beta}_p)$ is 0:

$$\lambda_{max} = \max_j \left\{ \left| \frac{1}{v_j} \sum_{i=1}^{N_T} \widehat{w}_i \widetilde{X}_{ij} (\widetilde{Y}_i - \widetilde{X}_{i1} \widehat{\beta}_0) \right| \right\}, \quad j = 1, \dots, p \quad (27)$$

532 Following Friedman et al. [20], we choose $\tau \lambda_{max}$ to be the smallest value of tuning parameters
533 λ_{min} , and construct a sequence of K values decreasing from λ_{max} to λ_{min} on the log scale.
534 The defaults are set to $K = 100$, $\tau = 0.01$ if $n < p$ and $\tau = 0.001$ if $n \geq p$.

535 **5.3.5 Warm Starts**

536 The way in which we have derived the sequence of tuning parameters using the KKT con-
537 ditions, allows us to implement warm starts. That is, the solution $\widehat{\Theta}$ for λ_k is used as the
538 initial value $\Theta^{(0)}$ for λ_{k+1} . This strategy leads to computational speedups and has been
539 implemented in the `ggmix` R package.

540 **5.3.6 Prediction of the random effects**

541 We use an empirical Bayes approach (e.g. [61]) to predict the random effects \mathbf{b} . Let the
542 maximum a posteriori (MAP) estimate be defined as

$$\widehat{\mathbf{b}} = \arg \max_{\mathbf{b}} f(\mathbf{b} | \mathbf{Y}, \boldsymbol{\beta}, \eta, \sigma^2) \quad (28)$$

where, by using Bayes rule, $f(\mathbf{b}|\mathbf{Y}, \boldsymbol{\beta}, \eta, \sigma^2)$ can be expressed as

$$\begin{aligned} f(\mathbf{b}|\mathbf{Y}, \boldsymbol{\beta}, \eta, \sigma^2) &= \frac{f(\mathbf{Y}|\mathbf{b}, \boldsymbol{\beta}, \eta, \sigma^2)\pi(\mathbf{b}|\eta, \sigma^2)}{f(\mathbf{Y}|\boldsymbol{\beta}, \eta, \sigma^2)} \\ &\propto f(\mathbf{Y}|\mathbf{b}, \boldsymbol{\beta}, \eta, \sigma^2)\pi(\mathbf{b}|\eta, \sigma^2) \\ &\propto \exp \left\{ -\frac{1}{2\sigma^2}(\mathbf{Y} - \mathbf{X}\boldsymbol{\beta} - \mathbf{b})^T(\mathbf{Y} - \mathbf{X}\boldsymbol{\beta} - \mathbf{b}) - \frac{1}{2\eta\sigma^2}\mathbf{b}^T\boldsymbol{\Phi}^{-1}\mathbf{b} \right\} \\ &= \exp \left\{ -\frac{1}{2\sigma^2} \left[(\mathbf{Y} - \mathbf{X}\boldsymbol{\beta} - \mathbf{b})^T(\mathbf{Y} - \mathbf{X}\boldsymbol{\beta} - \mathbf{b}) + \frac{1}{\eta}\mathbf{b}^T\boldsymbol{\Phi}^{-1}\mathbf{b} \right] \right\} \end{aligned} \quad (29)$$

Solving for (28) is equivalent to minimizing the exponent in (29):

$$\hat{\mathbf{b}} = \arg \min_{\mathbf{b}} \left\{ (\mathbf{Y} - \mathbf{X}\boldsymbol{\beta} - \mathbf{b})^T(\mathbf{Y} - \mathbf{X}\boldsymbol{\beta} - \mathbf{b}) + \frac{1}{\eta}\mathbf{b}^T\boldsymbol{\Phi}^{-1}\mathbf{b} \right\} \quad (30)$$

Taking the derivative of (30) with respect to \mathbf{b} and setting it to 0 we get:

$$\begin{aligned} 0 &= -2(\mathbf{Y} - \mathbf{X}\boldsymbol{\beta} - \mathbf{b}) + \frac{2}{\eta}\boldsymbol{\Phi}^{-1}\mathbf{b} \\ &= -(\mathbf{Y} - \mathbf{X}\boldsymbol{\beta}) + \mathbf{b} + \left(\frac{1}{\eta}\boldsymbol{\Phi}^{-1} \right) \mathbf{b} \\ (\mathbf{Y} - \mathbf{X}\boldsymbol{\beta}) &= \left(\mathbf{I}_{N_T \times N_T} + \frac{1}{\eta}\boldsymbol{\Phi}^{-1} \right) \mathbf{b} \\ \hat{\mathbf{b}} &= \left(\mathbf{I}_{N_T \times N_T} + \frac{1}{\hat{\eta}}\boldsymbol{\Phi}^{-1} \right)^{-1} (\mathbf{Y} - \mathbf{X}\hat{\boldsymbol{\beta}}) \\ &= \left(\mathbf{I}_{N_T \times N_T} + \frac{1}{\hat{\eta}}\mathbf{U}\mathbf{D}^{-1}\mathbf{U}^T \right)^{-1} (\mathbf{Y} - \mathbf{X}\hat{\boldsymbol{\beta}}) \end{aligned} \quad (31)$$

543 where $(\hat{\boldsymbol{\beta}}, \hat{\eta})$ are the estimates obtained from Algorithm 1.

544 5.3.7 Phenotype prediction

545 Here we describe the method used for predicting the unobserved phenotype \mathbf{Y}^* in a set of
 546 individuals with predictor set \mathbf{X}^* that were not used in the model training e.g. a testing
 547 set. Let q denote the number of observations in the testing set and $N - q$ the number of
 548 observations in the training set. We assume that a `gmmix` model has been fit on a set of

549 training individuals with observed phenotype \mathbf{Y} and predictor set \mathbf{X} . We further assume
 550 that \mathbf{Y} and \mathbf{Y}^* are jointly multivariate Normal:

$$\begin{bmatrix} \mathbf{Y}^* \\ \mathbf{Y} \end{bmatrix} \sim \mathcal{N} \left(\begin{bmatrix} \boldsymbol{\mu}_{1(q \times 1)} \\ \boldsymbol{\mu}_{2(N-q) \times 1} \end{bmatrix}, \begin{bmatrix} \boldsymbol{\Sigma}_{11(q \times q)} & \boldsymbol{\Sigma}_{12_{q \times (N-q)}} \\ \boldsymbol{\Sigma}_{21_{(N-q) \times q}} & \boldsymbol{\Sigma}_{22_{(N-q) \times (N-q)}} \end{bmatrix} \right) \quad (32)$$

551 Then, from standard multivariate Normal theory, the conditional distribution $\mathbf{Y}^* | \mathbf{Y}, \eta, \sigma^2, \boldsymbol{\beta}, \mathbf{X}, \mathbf{X}^*$
 552 is $\mathcal{N}(\boldsymbol{\mu}^*, \boldsymbol{\Sigma}^*)$ where

$$\boldsymbol{\mu}^* = \boldsymbol{\mu}_1 + \boldsymbol{\Sigma}_{12} \boldsymbol{\Sigma}_{22}^{-1} (\mathbf{Y} - \boldsymbol{\mu}_2) \quad (33)$$

$$\boldsymbol{\Sigma}^* = \boldsymbol{\Sigma}_{11} - \boldsymbol{\Sigma}_{12} \boldsymbol{\Sigma}_{22}^{-1} \boldsymbol{\Sigma}_{21} \quad (34)$$

553 The phenotype prediction is thus given by:

$$\boldsymbol{\mu}_{q \times 1}^* = \mathbf{X}^* \boldsymbol{\beta} + \frac{1}{\sigma^2} \boldsymbol{\Sigma}_{12} \mathbf{V}^{-1} (\mathbf{Y} - \mathbf{X} \boldsymbol{\beta}) \quad (35)$$

$$= \mathbf{X}^* \boldsymbol{\beta} + \frac{1}{\sigma^2} \boldsymbol{\Sigma}_{12} \mathbf{U} \tilde{\mathbf{D}}^{-1} \mathbf{U}^T (\mathbf{Y} - \mathbf{X} \boldsymbol{\beta}) \quad (36)$$

$$= \mathbf{X}^* \boldsymbol{\beta} + \frac{1}{\sigma^2} \boldsymbol{\Sigma}_{12} \mathbf{U} \tilde{\mathbf{D}}^{-1} (\tilde{\mathbf{Y}} - \tilde{\mathbf{X}} \boldsymbol{\beta}) \quad (37)$$

$$= \mathbf{X}^* \boldsymbol{\beta} + \frac{1}{\sigma^2} \eta \sigma^2 \boldsymbol{\Phi}^* \mathbf{U} \tilde{\mathbf{D}}^{-1} (\tilde{\mathbf{Y}} - \tilde{\mathbf{X}} \boldsymbol{\beta}) \quad (38)$$

$$= \mathbf{X}^* \boldsymbol{\beta} + \eta \boldsymbol{\Phi}^* \mathbf{U} \tilde{\mathbf{D}}^{-1} (\tilde{\mathbf{Y}} - \tilde{\mathbf{X}} \boldsymbol{\beta}) \quad (39)$$

554 where $\boldsymbol{\Phi}^*$ is the $q \times (N - q)$ covariance matrix between the testing and training individu-
 555 als.

556 5.3.8 Choice of the optimal tuning parameter

557 In order to choose the optimal value of the tuning parameter λ , we use the generalized
558 information criterion [62] (GIC):

$$GIC_\lambda = -2\ell(\hat{\boldsymbol{\beta}}, \hat{\sigma}^2, \hat{\eta}) + a_n \cdot \hat{df}_\lambda \quad (40)$$

559 where \hat{df}_λ is the number of non-zero elements in $\hat{\boldsymbol{\beta}}_\lambda$ [63] plus two (representing the variance
560 parameters η and σ^2). Several authors have used this criterion for variable selection in mixed
561 models with $a_n = \log N_T$ [57, 64], which corresponds to the BIC. We instead choose the high-
562 dimensional BIC [65] given by $a_n = \log(\log(N_T)) * \log(p)$. This is the default choice in our
563 `ggmix` R package, though the interface is flexible to allow the user to select their choice of
564 a_n .

565 **Availability of data and material**

- 566 1. The UK Biobank data is available upon successful project application.
- 567 2. The GAW20 data is freely available upon request from <https://www.gaworkshop.org/data-sets>.
- 569 3. Mouse cross data is available from GitHub at <https://github.com/sahirbhatnagar/ggmix/blob/master/RealData/mice.RData>.
- 571 4. The entire simulation study is reproducible. Source code available at <https://github.com/sahirbhatnagar/ggmix/tree/master/simulation>. This includes scripts for ggmix, lasso and twostep methods.
- 574 5. The R package `ggmix` is freely available from CRAN at <https://cran.r-project.org/package=ggmix>.
- 576 6. A website describing how to use the package is available at <https://sahirbhatnagar.com/ggmix/>.

578 **Competing interests**

579 The authors declare that they have no competing interests.

580 **Author's contributions**

581 SRB, KO, YY and CMTG conceived the idea. SRB developed the algorithms, software
582 and simulation study. TL completed the real data analysis. ES and JCLO provided data
583 and interpretations. SRB, TL and CMTG wrote a draft of the manuscript then all authors
584 edited, read and approved the final manuscript.

585 Acknowledgements

586 SRB was supported by the Ludmer Centre for Neuroinformatics and Mental Health and
587 the Canadian Institutes for Health Research PJT 148620. This research was enabled in
588 part by support provided by Calcul Québec (www.calculquebec.ca) and Compute Canada
589 (www.computecanada.ca). The funders had no role in study design, data collection and
590 analysis, decision to publish, or preparation of the manuscript.

591 Supporting Information

592 Contains the following sections:

593 **A Block Coordinate Descent Algorithm** - a detailed description of the algorithm
594 used to fit our `gmmix` model.

595 **B Additional Real Data Analysis Results** - supporting information for the GAW20
596 and UK Biobank analyses

597 **C gmmix Package Showcase** - a vignette describing how to use our `gmmix` R package

598 References

599 [1] Manolio TA, Collins FS, Cox NJ, Goldstein DB, Hindorff LA, Hunter DJ, et al. Finding
600 the missing heritability of complex diseases. *Nature*. 2009;461(7265):747. [3](#), [25](#)

601 [2] Yang J, Benyamin B, McEvoy BP, Gordon S, Henders AK, Nyholt DR, et al. Common
602 SNPs explain a large proportion of the heritability for human height. *Nature genetics*.
603 2010;42(7):565. [3](#)

604 [3] Astle W, Balding DJ, et al. Population structure and cryptic relatedness in genetic
605 association studies. *Statistical Science*. 2009;24(4):451–471. [3](#), [4](#)

- 606 [4] Song M, Hao W, Storey JD. Testing for genetic associations in arbitrarily structured
607 populations. *Nature genetics*. 2015;47(5):550–554. 3
- 608 [5] Marchini J, Cardon LR, Phillips MS, Donnelly P. The effects of human population
609 structure on large genetic association studies. *Nature genetics*. 2004;36(5):512. 3
- 610 [6] Hoggart CJ, Whittaker JC, De Iorio M, Balding DJ. Simultaneous analysis of all SNPs in
611 genome-wide and re-sequencing association studies. *PLoS genetics*. 2008;4(7):e1000130.
612 4, 22
- 613 [7] Li J, Das K, Fu G, Li R, Wu R. The Bayesian lasso for genome-wide association studies.
614 *Bioinformatics*. 2010;27(4):516–523. 4
- 615 [8] Lippert C, Listgarten J, Liu Y, Kadie CM, Davidson RI, Heckerman D. FaST linear
616 mixed models for genome-wide association studies. *Nature methods*. 2011;8(10):833–
617 835. 4, 7, 22, 23
- 618 [9] Kang HM, Sul JH, Zaitlen NA, Kong Sy, Freimer NB, Sabatti C, et al. Variance
619 component model to account for sample structure in genome-wide association studies.
620 *Nature genetics*. 2010;42(4):348. 4
- 621 [10] Yu J, Pressoir G, Briggs WH, Bi IV, Yamasaki M, Doebley JF, et al. A unified mixed-
622 model method for association mapping that accounts for multiple levels of relatedness.
623 *Nature genetics*. 2006;38(2):203. 4
- 624 [11] Eu-Ahsunthornwattana J, Miller EN, Fakiola M, Jeronimo SM, Blackwell JM, Cordell
625 HJ, et al. Comparison of methods to account for relatedness in genome-wide association
626 studies with family-based data. *PLoS Genet*. 2014;10(7):e1004445. 4
- 627 [12] Price AL, Patterson NJ, Plenge RM, Weinblatt ME, Shadick NA, Reich D. Princi-
628 pal components analysis corrects for stratification in genome-wide association studies.
629 *Nature genetics*. 2006;38(8):904. 4

- [13] Oualkacha K, Dastani Z, Li R, Cingolani PE, Spector TD, Hammond CJ, et al. Adjusted sequence kernel association test for rare variants controlling for cryptic and family relatedness. *Genetic epidemiology*. 2013;37(4):366–376. [4](#), [5](#)
- [14] Cordell HJ, Clayton DG. A unified stepwise regression procedure for evaluating the relative effects of polymorphisms within a gene using case/control or family data: application to HLA in type 1 diabetes. *The American Journal of Human Genetics*. 2002;70(1):124–141. [4](#)
- [15] Rakitsch B, Lippert C, Stegle O, Borgwardt K. A Lasso multi-marker mixed model for association mapping with population structure correction. *Bioinformatics*. 2013;29(2):206–214. [4](#), [23](#), [25](#)
- [16] Wang D, Eskridge KM, Crossa J. Identifying QTLs and epistasis in structured plant populations using adaptive mixed LASSO. *Journal of agricultural, biological, and environmental statistics*. 2011;16(2):170–184. [4](#)
- [17] Tibshirani R. Regression shrinkage and selection via the lasso. *Journal of the Royal Statistical Society Series B (Methodological)*. 1996;p. 267–288. [4](#), [5](#)
- [18] Zou H. The adaptive lasso and its oracle properties. *Journal of the American statistical association*. 2006;101(476):1418–1429. [4](#)
- [19] Ding X, Su S, Nandakumar K, Wang X, Fardo DW. A 2-step penalized regression method for family-based next-generation sequencing association studies. In: *BMC proceedings*. vol. 8. BioMed Central; 2014. p. S25. [5](#)
- [20] Friedman J, Hastie T, Tibshirani R. Regularization paths for generalized linear models via coordinate descent. *Journal of statistical software*. 2010;33(1):1. [5](#), [6](#), [29](#), [34](#), [47](#)
- [21] Yang Y, Zou H. A fast unified algorithm for solving group-lasso penalize learning problems. *Statistics and Computing*. 2015;25(6):1129–1141. [5](#)

- 654 [22] Yang J, Zaitlen NA, Goddard ME, Visscher PM, Price AL. Advantages and pitfalls in
655 the application of mixed-model association methods. *Nature genetics*. 2014;46(2):100.
656 5, 24
- 657 [23] Zou H, Hastie T. Regularization and variable selection via the elastic net. *Journal of*
658 *the Royal Statistical Society: Series B (Statistical Methodology)*. 2005;67(2):301–320.
659 5
- 660 [24] Gilmour AR, Thompson R, Cullis BR. Average information REML: an efficient algo-
661 rithm for variance parameter estimation in linear mixed models. *Biometrics*. 1995;p.
662 1440–1450. 6
- 663 [25] Dandine-Roulland C. *gaston: Genetic Data Handling (QC, GRM, LD, PCA) and*
664 *Linear Mixed Models*; 2018. R package version 1.5.3. Available from: <https://CRAN.R-project.org/package=gaston>. 6
- 666 [26] Ochoa A, Storey JD. FST and kinship for arbitrary population structures I: Generalized
667 definitions. *bioRxiv*. 2016;. 8
- 668 [27] Ochoa A, Storey JD. FST and kinship for arbitrary population structures II: Method
669 of moments estimators. *bioRxiv*. 2016;. 8
- 670 [28] Reid S, Tibshirani R, Friedman J. A study of error variance estimation in lasso regres-
671 sion. *Statistica Sinica*. 2016;p. 35–67. 11
- 672 [29] Bycroft C, Freeman C, Petkova D, Band G, Elliott LT, Sharp K, et al. The UK Biobank
673 resource with deep phenotyping and genomic data. *Nature*. 2018;562(7726):203. 12
- 674 [30] Biobank U. Genotyping and quality control of UK Biobank, a large-scale, ex-
675 tensively phenotyped prospective resource. Available at biobank ctsu ox ac
676 uk/crystal/docs/genotyping_qc pdf Accessed April. 2015;1:2016. 12

- 677 [31] Manichaikul A, Mychaleckyj JC, Rich SS, Daly K, Sale M, Chen WM. Robust relation-
678 ship inference in genome-wide association studies. *Bioinformatics*. 2010;26(22):2867–
679 2873. [12](#)
- 680 [32] Yengo L, Sidorenko J, Kemper KE, Zheng Z, Wood AR, Weedon MN, et al. Meta-
681 analysis of genome-wide association studies for height and body mass index in 700000
682 individuals of European ancestry. *Human molecular genetics*. 2018;27(20):3641–3649.
683 [12, 13](#)
- 684 [33] McCarthy S, Das S, Kretzschmar W, Delaneau O, Wood AR, Teumer A, et al. A reference panel of 64,976 haplotypes for genotype imputation. *Nature genetics*.
685 2016;48(10):1279. [13](#)
- 687 [34] Zhou X, Carbonetto P, Stephens M. Polygenic modeling with Bayesian sparse linear
688 mixed models. *PLoS genetics*. 2013;9(2):e1003264. [13](#)
- 689 [35] Zhou X, Stephens M. Genome-wide efficient mixed-model analysis for association stud-
690 ies. *Nature genetics*. 2012;44(7):821. [13](#)
- 691 [36] Davey Smith G, Ebrahim S. ‘Mendelian randomization’: can genetic epidemiology con-
692 tribute to understanding environmental determinants of disease? *International journal
693 of epidemiology*. 2003;32(1):1–22. [14](#)
- 694 [37] Cherlin S, Howey RA, Cordell HJ. Using penalized regression to predict phenotype
695 from SNP data. In: *BMC proceedings*. vol. 12. BioMed Central; 2018. p. 38. [14](#)
- 696 [38] Zhou W, Lo SH. Analysis of genotype by methylation interactions through sparsity-
697 inducing regularized regression. In: *BMC proceedings*. vol. 12. BioMed Central; 2018.
698 p. 40. [14](#)
- 699 [39] Howey RA, Cordell HJ. Application of Bayesian networks to GAW20 genetic and blood
700 lipid data. In: *BMC proceedings*. vol. 12. BioMed Central; 2018. p. 19. [15](#)

- 701 [40] Thornton T, Tang H, Hoffmann TJ, Ochs-Balcom HM, Caan BJ, Risch N. Estimating kinship in admixed populations. *The American Journal of Human Genetics*.
702 2012;91(1):122–138. 15
- 703
- 704 [41] Alexander DH, Novembre J, Lange K. Fast model-based estimation of ancestry in
705 unrelated individuals. *Genome research*. 2009;19(9):1655–1664. 15
- 706
- 707 [42] Fortin A, Diez E, Rochefort D, Laroche L, Malo D, Rouleau GA, et al. Recombinant
708 congenic strains derived from A/J and C57BL/6J: a tool for genetic dissection of com-
plex traits. *Genomics*. 2001;74(1):21–35. 17
- 709
- 710 [43] Bennett BJ, Farber CR, Orozco L, Kang HM, Ghazalpour A, Siemers N, et al. A
711 high-resolution association mapping panel for the dissection of complex traits in mice.
712 *Genome research*. 2010;20(2):281–290. 17
- 713
- 714 [44] Flint J, Eskin E. Genome-wide association studies in mice. *Nature Reviews Genetics*.
715 2012;13(11):807. 17
- 716
- 717 [45] Cheng R, Lim JE, Samocha KE, Sokoloff G, Abney M, Skol AD, et al. Genome-wide
718 association studies and the problem of relatedness among advanced intercross lines and
719 other highly recombinant populations. *Genetics*. 2010;185(3):1033–1044. 17
- 720
- 721 [46] Di Pietrantonio T, Hernandez C, Girard M, Verville A, Orlova M, Belley A, et al.
722 Strain-specific differences in the genetic control of two closely related mycobacteria.
723 *PLoS pathogens*. 2010;6(10):e1001169. 17, 18
- 724
- 725 [47] Wang H, Lengerich BJ, Aragam B, Xing EP. Precision Lasso: accounting for cor-
726 relations and linear dependencies in high-dimensional genomic data. *Bioinformatics*.
727 2018;35(7):1181–1187. 19, 23
- 728
- 729 [48] Sohrabi Y, Havelková H, Kobets T, Šíma M, Volkova V, Grekov I, et al. Mapping the

- 724 Genes for Susceptibility and Response to *Leishmania tropica* in Mouse. PLoS neglected
725 tropical diseases. 2013;7(7):e2282. 19
- 726 [49] Jackson AU, Fornés A, Galecki A, Miller RA, Burke DT. Multiple-trait quantitative
727 trait loci analysis using a large mouse sibship. Genetics. 1999;151(2):785–795. 19
- 728 [50] C Stern1 M, Benavides F, A Klingelberger E, J Conti2 C. Allelotype analysis of chemi-
729 cally induced squamous cell carcinomas in F1 hybrids of two inbred mouse strains with
730 different susceptibility to tumor progression. Carcinogenesis. 2000;21(7):1297–1301. 19
- 731 [51] Lasko D, Cavenee W, Nordenskjöld M. Loss of constitutional heterozygosity in human
732 cancer. Annual review of genetics. 1991;25(1):281–314. 19
- 733 [52] Loh PR, Tucker G, Bulik-Sullivan BK, Vilhjalmsson BJ, Finucane HK, Salem RM, et al.
734 Efficient Bayesian mixed-model analysis increases association power in large cohorts.
735 Nature genetics. 2015;47(3):284. 22
- 736 [53] Allen N, Sudlow C, Downey P, Peakman T, Danesh J, Elliott P, et al. UK Biobank:
737 Current status and what it means for epidemiology. Health Policy and Technology.
738 2012;1(3):123–126. 23
- 739 [54] Zeng Y, Breheny P. The biglasso package: a memory-and computation-efficient solver
740 for lasso model fitting with big data in R. arXiv preprint arXiv:170105936. 2017;. 24
- 741 [55] Spain SL, Barrett JC. Strategies for fine-mapping complex traits. Human molecular
742 genetics. 2015;24(R1):R111–R119. 24
- 743 [56] Pirinen M, Donnelly P, Spencer CC, et al. Efficient computation with a linear mixed
744 model on large-scale data sets with applications to genetic studies. The Annals of
745 Applied Statistics. 2013;7(1):369–390. 25, 26

- 746 [57] Schelldorfer J, Bühlmann P, DE G, VAN S. Estimation for High-Dimensional Lin-
747 ear Mixed-Effects Models Using L1-Penalization. Scandinavian Journal of Statistics.
748 2011;38(2):197–214. [29](#), [37](#), [47](#)
- 749 [58] Tseng P, Yun S. A coordinate gradient descent method for nonsmooth separable mini-
750 mization. Mathematical Programming. 2009;117(1):387–423. [29](#), [47](#), [50](#)
- 751 [59] Meier L, Van De Geer S, Bühlmann P. The group lasso for logistic regression. Journal
752 of the Royal Statistical Society: Series B (Statistical Methodology). 2008;70(1):53–71.
753 [29](#), [47](#)
- 754 [60] Byrd RH, Lu P, Nocedal J, Zhu C. A limited memory algorithm for bound constrained
755 optimization. SIAM Journal on Scientific Computing. 1995;16(5):1190–1208. [31](#)
- 756 [61] Wakefield J. Bayesian and frequentist regression methods. Springer Science & Business
757 Media; 2013. [34](#)
- 758 [62] Nishii R. Asymptotic properties of criteria for selection of variables in multiple regres-
759 sion. The Annals of Statistics. 1984;p. 758–765. [37](#)
- 760 [63] Zou H, Hastie T, Tibshirani R, et al. On the “degrees of freedom” of the lasso. The
761 Annals of Statistics. 2007;35(5):2173–2192. [37](#)
- 762 [64] Bondell HD, Krishna A, Ghosh SK. Joint Variable Selection for Fixed and Random
763 Effects in Linear Mixed-Effects Models. Biometrics. 2010;66(4):1069–1077. [37](#)
- 764 [65] Fan Y, Tang CY. Tuning parameter selection in high dimensional penalized likeli-
765 hood. Journal of the Royal Statistical Society: Series B (Statistical Methodology).
766 2013;75(3):531–552. [37](#)
- 767 [66] Xie Y. Dynamic Documents with R and knitr. vol. 29. CRC Press; 2015. [57](#)

768 A Block Coordinate Descent Algorithm

769 We use a general purpose block coordinate descent algorithm (CGD) [58] to solve (16). At
 770 each iteration, the algorithm approximates the negative log-likelihood $f(\cdot)$ in $Q_\lambda(\cdot)$ by a
 771 strictly convex quadratic function and then applies block coordinate decent to generate a
 772 decent direction followed by an inexact line search along this direction [58]. For continuously
 773 differentiable $f(\cdot)$ and convex and block-separable $P(\cdot)$ (i.e. $P(\beta) = \sum_i P_i(\beta_i)$), [58] show
 774 that the solution generated by the CGD method is a stationary point of $Q_\lambda(\cdot)$ if the coor-
 775 dinates are updated in a Gauss-Seidel manner i.e. $Q_\lambda(\cdot)$ is minimized with respect to one
 776 parameter while holding all others fixed. The CGD algorithm can thus be run in parallel and
 777 therefore suited for large p settings. It has been successfully applied in fixed effects models
 778 (e.g. [59], [20]) and [57] for mixed models with an ℓ_1 penalty. Following Tseng and Yun [58],
 779 the CGD algorithm is given by Algorithm 2.

780 The Armijo rule is defined as follows [58]:

Choose $\alpha_{init}^{(k)} > 0$ and let $\alpha^{(k)}$ be the largest element of $\{\alpha_{init}^k \delta^r\}_{r=0,1,2,\dots}$ satisfying

$$Q_\lambda(\Theta_j^{(k)} + \alpha^{(k)} d^{(k)}) \leq Q_\lambda(\Theta_j^{(k)}) + \alpha^{(k)} \varrho \Delta^{(k)} \quad (45)$$

where $0 < \delta < 1$, $0 < \varrho < 1$, $0 \leq \gamma < 1$ and

$$\Delta^{(k)} := \nabla f(\Theta_j^{(k)}) d^{(k)} + \gamma (d^{(k)})^2 H_{jj}^{(k)} + \lambda P(\Theta_j^{(k)} + d^{(k)}) - \lambda P(\Theta_j^{(k)}) \quad (46)$$

781 Common choices for the constants are $\delta = 0.1$, $\varrho = 0.001$, $\gamma = 0$, $\alpha_{init}^{(k)} = 1$ for all k [57].

783 Below we detail the specifics of Algorithm 2 for the ℓ_1 penalty.

Algorithm 2: Coordinate Gradient Descent Algorithm to solve (16)

Set the iteration counter $k \leftarrow 0$ and choose initial values for the parameter vector

$$\Theta^{(0)};$$

repeat

 Approximate the Hessian $\nabla^2 f(\Theta^{(k)})$ by a symmetric matrix $H^{(k)}$:

$$H^{(k)} = \text{diag} \left[\min \left\{ \max \left\{ \left[\nabla^2 f(\Theta^{(k)}) \right]_{jj}, c_{min} \right\} c_{max} \right\} \right]_{j=1,\dots,p} \quad (41)$$

for $j = 1, \dots, p$ **do**

 Solve the descent direction $d^{(k)} := d_{H^{(k)}}(\Theta_j^{(k)})$;

if $\Theta_j^{(k)} \in \{\beta_1, \dots, \beta_p\}$ **then**

$$d_{H^{(k)}}(\Theta_j^{(k)}) \leftarrow \arg \min_d \left\{ \nabla f(\Theta_j^{(k)})d + \frac{1}{2}d^2 H_{jj}^{(k)} + \lambda P(\Theta_j^{(k)} + d) \right\} \quad (42)$$

end
end

Choose a stepsize;

$$\alpha_j^{(k)} \leftarrow \text{line search given by the Armijo rule}$$

Update;

$$\widehat{\Theta}_j^{(k+1)} \leftarrow \widehat{\Theta}_j^{(k)} + \alpha_j^{(k)} d^{(k)}$$

Update;

$$\widehat{\eta}^{(k+1)} \leftarrow \arg \min_{\eta} \frac{1}{2} \sum_{i=1}^{N_T} \log(1 + \eta(\Lambda_i - 1)) + \frac{1}{2\sigma^2(k)} \sum_{i=1}^{N_T} \frac{\left(\widetilde{Y}_i - \sum_{j=0}^p \widetilde{X}_{ij+1} \beta_j^{(k+1)} \right)^2}{1 + \eta(\Lambda_i - 1)} \quad (43)$$

Update;

$$\widehat{\sigma^2}^{(k+1)} \leftarrow \frac{1}{N_T} \sum_{i=1}^{N_T} \frac{\left(\widetilde{Y}_i - \sum_{j=0}^p \widetilde{X}_{ij+1} \beta_j^{(k+1)} \right)^2}{1 + \eta^{(k+1)}(\Lambda_i - 1)} \quad (44)$$

$$k \leftarrow k + 1$$

until convergence criterion is satisfied;

⁷⁸⁴ **A.1 ℓ_1 penalty**

⁷⁸⁵ The objective function is given by

$$Q_\lambda(\Theta) = f(\Theta) + \lambda|\beta| \quad (47)$$

⁷⁸⁶ **A.1.1 Descent Direction**

⁷⁸⁷ For simplicity, we remove the iteration counter (k) from the derivation below.

⁷⁸⁸ For $\Theta_j^{(k)} \in \{\beta_1, \dots, \beta_p\}$, let

$$d_H(\Theta_j) = \arg \min_d G(d) \quad (48)$$

⁷⁸⁹ where

$$G(d) = \nabla f(\Theta_j)d + \frac{1}{2}d^2 H_{jj} + \lambda|\Theta_j + d|$$

⁷⁹⁰ Since $G(d)$ is not differentiable at $-\Theta_j$, we calculate the subdifferential $\partial G(d)$ and search

⁷⁹¹ for d with $0 \in \partial G(d)$:

$$\partial G(d) = \nabla f(\Theta_j) + dH_{jj} + \lambda u \quad (49)$$

⁷⁹² where

$$u = \begin{cases} 1 & \text{if } d > -\Theta_j \\ -1 & \text{if } d < -\Theta_j \\ [-1, 1] & \text{if } d = \Theta_j \end{cases} \quad (50)$$

⁷⁹³ We consider each of the three cases in (49) below

1. $d > -\Theta_j$

$$\partial G(d) = \nabla f(\Theta_j) + dH_{jj} + \lambda = 0$$

$$d = \frac{-(\nabla f(\Theta_j) + \lambda)}{H_{jj}}$$

Since $\lambda > 0$ and $H_{jj} > 0$, we have

$$\frac{-(\nabla f(\Theta_j) - \lambda)}{H_{jj}} > \frac{-(\nabla f(\Theta_j) + \lambda)}{H_{jj}} = d \stackrel{\text{def}}{>} -\Theta_j$$

The solution can be written compactly as

$$d = \text{mid} \left\{ \frac{-(\nabla f(\Theta_j) - \lambda)}{H_{jj}}, -\Theta_j, \frac{-(\nabla f(\Theta_j) + \lambda)}{H_{jj}} \right\}$$

794 where $\text{mid} \{a, b, c\}$ denotes the median (mid-point) of a, b, c [58].

2. $d < -\Theta_j$

$$\begin{aligned} \partial G(d) &= \nabla f(\Theta_j) + dH_{jj} - \lambda = 0 \\ d &= \frac{-(\nabla f(\Theta_j) - \lambda)}{H_{jj}} \end{aligned}$$

Since $\lambda > 0$ and $H_{jj} > 0$, we have

$$\frac{-(\nabla f(\Theta_j) + \lambda)}{H_{jj}} < \frac{-(\nabla f(\Theta_j) - \lambda)}{H_{jj}} = d \stackrel{\text{def}}{<} -\Theta_j$$

Again, the solution can be written compactly as

$$d = \text{mid} \left\{ \frac{-(\nabla f(\Theta_j) - \lambda)}{H_{jj}}, -\Theta_j, \frac{-(\nabla f(\Theta_j) + \lambda)}{H_{jj}} \right\}$$

3. $d_j = -\Theta_j$

There exists $u \in [-1, 1]$ such that

$$\begin{aligned} \partial G(d) &= \nabla f(\Theta_j) + dH_{jj} + \lambda u = 0 \\ d &= \frac{-(\nabla f(\Theta_j) + \lambda u)}{H_{jj}} \end{aligned}$$

For $-1 \leq u \leq 1$, $\lambda > 0$ and $H_{jj} > 0$ we have

$$\frac{-(\nabla f(\Theta_j) + \lambda)}{H_{jj}} \leq d \stackrel{\text{def}}{=} -\Theta_j \leq \frac{-(\nabla f(\Theta_j) - \lambda)}{H_{jj}}$$

The solution can again be written compactly as

$$d = \text{mid} \left\{ \frac{-(\nabla f(\Theta_j) - \lambda)}{H_{jj}}, -\Theta_j, \frac{-(\nabla f(\Theta_j) + \lambda)}{H_{jj}} \right\}$$

795 We see all three cases lead to the same solution for (48). Therefore the descent direction for
796 $\Theta_j^{(k)} \in \{\beta_1, \dots, \beta_p\}$ for the ℓ_1 penalty is given by

$$d = \text{mid} \left\{ \frac{-(\nabla f(\beta_j) - \lambda)}{H_{jj}}, -\beta_j, \frac{-(\nabla f(\beta_j) + \lambda)}{H_{jj}} \right\} \quad (51)$$

797 **A.1.2 Solution for the β parameter**

798 If the Hessian $\nabla^2 f(\Theta^{(k)}) > 0$ then $H^{(k)}$ defined in (41) is equal to $\nabla^2 f(\Theta^{(k)})$. Using $\alpha_{init} = 1$,
799 the largest element of $\{\alpha_{init}^{(k)} \delta^r\}_{r=0,1,2,\dots}$ satisfying the Armijo Rule inequality is reached for
800 $\alpha^{(k)} = \alpha_{init}^{(k)} \delta^0 = 1$. The Armijo rule update for the β parameter is then given by

$$\beta_j^{(k+1)} \leftarrow \beta_j^{(k)} + d^{(k)}, \quad j = 1, \dots, p \quad (52)$$

801 Substituting the descent direction given by (51) into (52) we get

$$\beta_j^{(k+1)} = \text{mid} \left\{ \beta_j^{(k)} + \frac{-(\nabla f(\beta_j^{(k)}) - \lambda)}{H_{jj}}, 0, \beta_j^{(k)} + \frac{-(\nabla f(\beta_j^{(k)}) + \lambda)}{H_{jj}} \right\} \quad (53)$$

802 We can further simplify this expression. Let

$$w_i := \frac{1}{\sigma^2 (1 + \eta(\Lambda_i - 1))} \quad (54)$$

Re-write the part depending on β of the negative log-likelihood in (14) as

$$g(\boldsymbol{\beta}^{(k)}) = \frac{1}{2} \sum_{i=1}^{N_T} w_i \left(\tilde{Y}_i - \sum_{\ell \neq j} \tilde{X}_{i\ell} \beta_\ell^{(k)} - \tilde{X}_{ij} \beta_j^{(k)} \right)^2 \quad (55)$$

The gradient and Hessian are given by

$$\nabla f(\beta_j^{(k)}) := \frac{\partial}{\partial \beta_j^{(k)}} g(\boldsymbol{\beta}^{(k)}) = - \sum_{i=1}^{N_T} w_i \tilde{X}_{ij} \left(\tilde{Y}_i - \sum_{\ell \neq j} \tilde{X}_{i\ell} \beta_\ell^{(k)} - \tilde{X}_{ij} \beta_j^{(k)} \right) \quad (56)$$

$$H_{jj} := \frac{\partial^2}{\partial \beta_j^{(k)} \partial \beta_j^{(k)}} g(\boldsymbol{\beta}^{(k)}) = \sum_{i=1}^{N_T} w_i \tilde{X}_{ij}^2 \quad (57)$$

Substituting (56) and (57) into $\beta_j^{(k)} + \frac{-(\nabla f(\beta_j^{(k)}) - \lambda)}{H_{jj}}$

$$\begin{aligned} & \beta_j^{(k)} + \frac{\sum_{i=1}^{N_T} w_i \tilde{X}_{ij} \left(\tilde{Y}_i - \sum_{\ell \neq j} \tilde{X}_{i\ell} \beta_\ell^{(k)} - \tilde{X}_{ij} \beta_j^{(k)} \right) + \lambda}{\sum_{i=1}^{N_T} w_i \tilde{X}_{ij}^2} \\ &= \beta_j^{(k)} + \frac{\sum_{i=1}^{N_T} w_i \tilde{X}_{ij} \left(\tilde{Y}_i - \sum_{\ell \neq j} \tilde{X}_{i\ell} \beta_\ell^{(k)} \right) + \lambda}{\sum_{i=1}^{N_T} w_i \tilde{X}_{ij}^2} - \frac{\sum_{i=1}^{N_T} w_i \tilde{X}_{ij}^2 \beta_j^{(k)}}{\sum_{i=1}^{N_T} w_i \tilde{X}_{ij}^2} \\ &= \frac{\sum_{i=1}^{N_T} w_i \tilde{X}_{ij} \left(\tilde{Y}_i - \sum_{\ell \neq j} \tilde{X}_{i\ell} \beta_\ell^{(k)} \right) + \lambda}{\sum_{i=1}^{N_T} w_i \tilde{X}_{ij}^2} \end{aligned} \quad (58)$$

Similarly, substituting (56) and (57) in $\beta_j^{(k)} + \frac{-(\nabla f(\beta_j^{(k)}) + \lambda)}{H_{jj}}$ we get

$$\frac{\sum_{i=1}^{N_T} w_i \tilde{X}_{ij} \left(\tilde{Y}_i - \sum_{\ell \neq j} \tilde{X}_{i\ell} \beta_\ell^{(k)} \right) - \lambda}{\sum_{i=1}^{N_T} w_i \tilde{X}_{ij}^2} \quad (59)$$

Finally, substituting (58) and (59) into (53) we get

$$\begin{aligned}\beta_j^{(k+1)} &= \text{mid} \left\{ \frac{\sum_{i=1}^{N_T} w_i \tilde{X}_{ij} \left(\tilde{Y}_i - \sum_{\ell \neq j} \tilde{X}_{i\ell} \beta_\ell^{(k)} \right) - \lambda}{\sum_{i=1}^{N_T} w_i \tilde{X}_{ij}^2}, 0, \frac{\sum_{i=1}^{N_T} w_i \tilde{X}_{ij} \left(\tilde{Y}_i - \sum_{\ell \neq j} \tilde{X}_{i\ell} \beta_\ell^{(k)} \right) + \lambda}{\sum_{i=1}^{N_T} w_i \tilde{X}_{ij}^2} \right\} \\ &= \frac{\mathcal{S}_\lambda \left(\sum_{i=1}^{N_T} w_i \tilde{X}_{ij} \left(\tilde{Y}_i - \sum_{\ell \neq j} \tilde{X}_{i\ell} \beta_\ell^{(k)} \right) \right)}{\sum_{i=1}^{N_T} w_i \tilde{X}_{ij}^2}\end{aligned}\tag{60}$$

Where $\mathcal{S}_\lambda(x)$ is the soft-thresholding operator

$$\mathcal{S}_\lambda(x) = \text{sign}(x)(|x| - \lambda)_+$$

$\text{sign}(x)$ is the signum function

$$\text{sign}(x) = \begin{cases} -1 & x < 0 \\ 0 & x = 0 \\ 1 & x > 0 \end{cases}$$

and $(x)_+ = \max(x, 0)$.

805 **B Additional Real Data Analysis Results**

806 **B.1 Distribution of SNPs used in UK Biobank analysis**

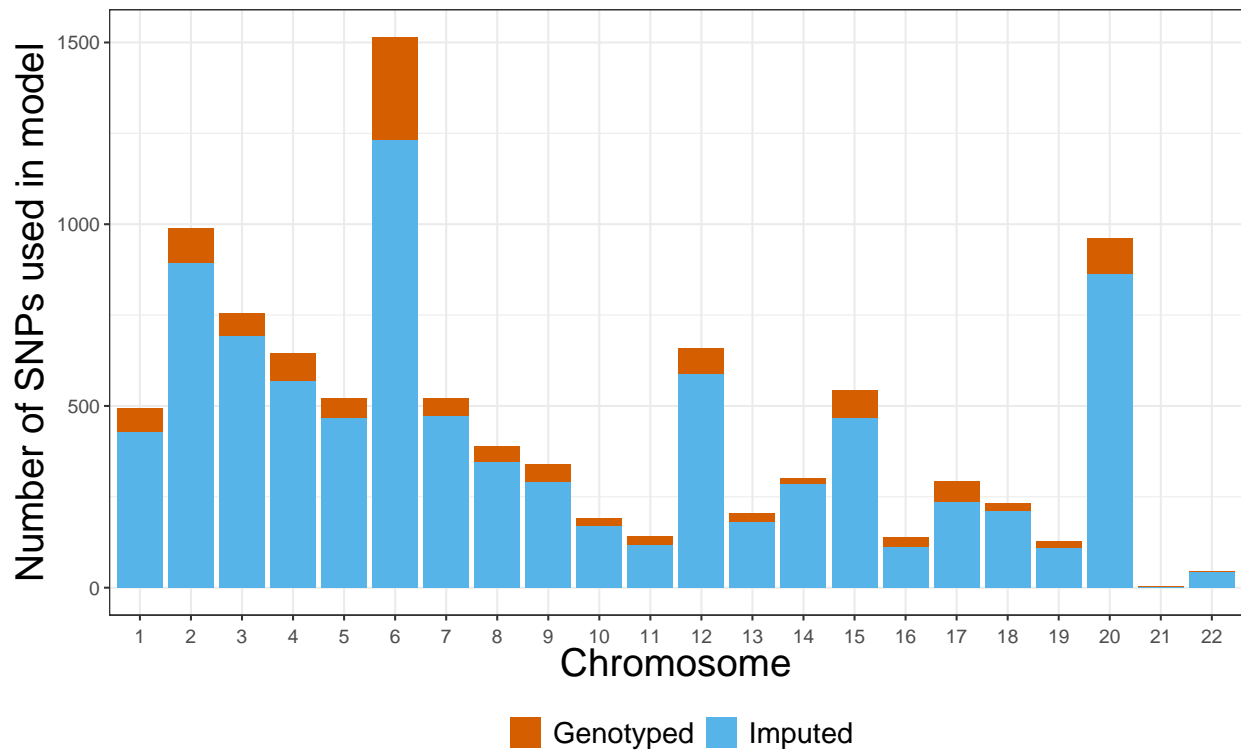


Figure B.1: Distribution of SNPs used in UK Biobank analysis by chromosome and whether or not the SNP was imputed.

807 **B.2 LD structure among the markers in the GAW20 and the mouse**
 808 **dataset**

809 We illustrate the LD structure among the markers in the GAW20 dataset and the mouse
 810 dataset separately in Figures B.2 and B.3, respectively. In Figure B.2, we show the pairwise
 811 r^2 for 655 SNPs within a 1Mb-window around the causal SNP rs9661059 (indicated) that we
 812 focused on. The dotplot above the heatmap denotes r^2 between each SNP and the causal
 813 SNP. It is clear that although strong correlation does exist between some SNPs, none of these
 814 nearby SNPs is correlated with the causal SNP. The only dot denoting an $r^2 = 1$ represents
 815 the causal SNP itself.

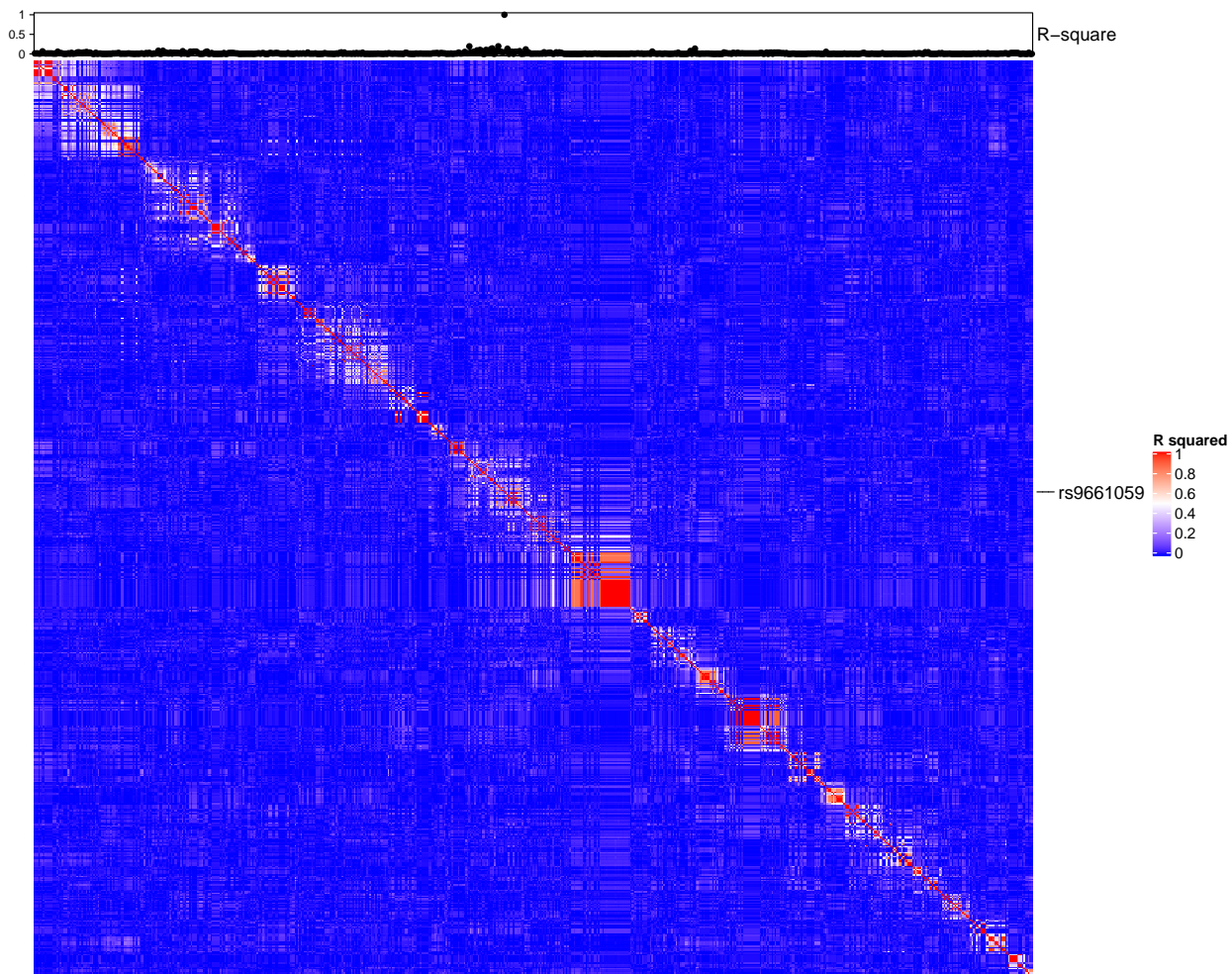


Figure B.2: LD structure among the markers in the GAW20 dataset

- 816 In Figure B.3, we show the pairwise r^2 for all microsatellite markers in the mouse dataset.
817 It is clear that many markers are considerably strongly correlated with each other, as we
818 expected.

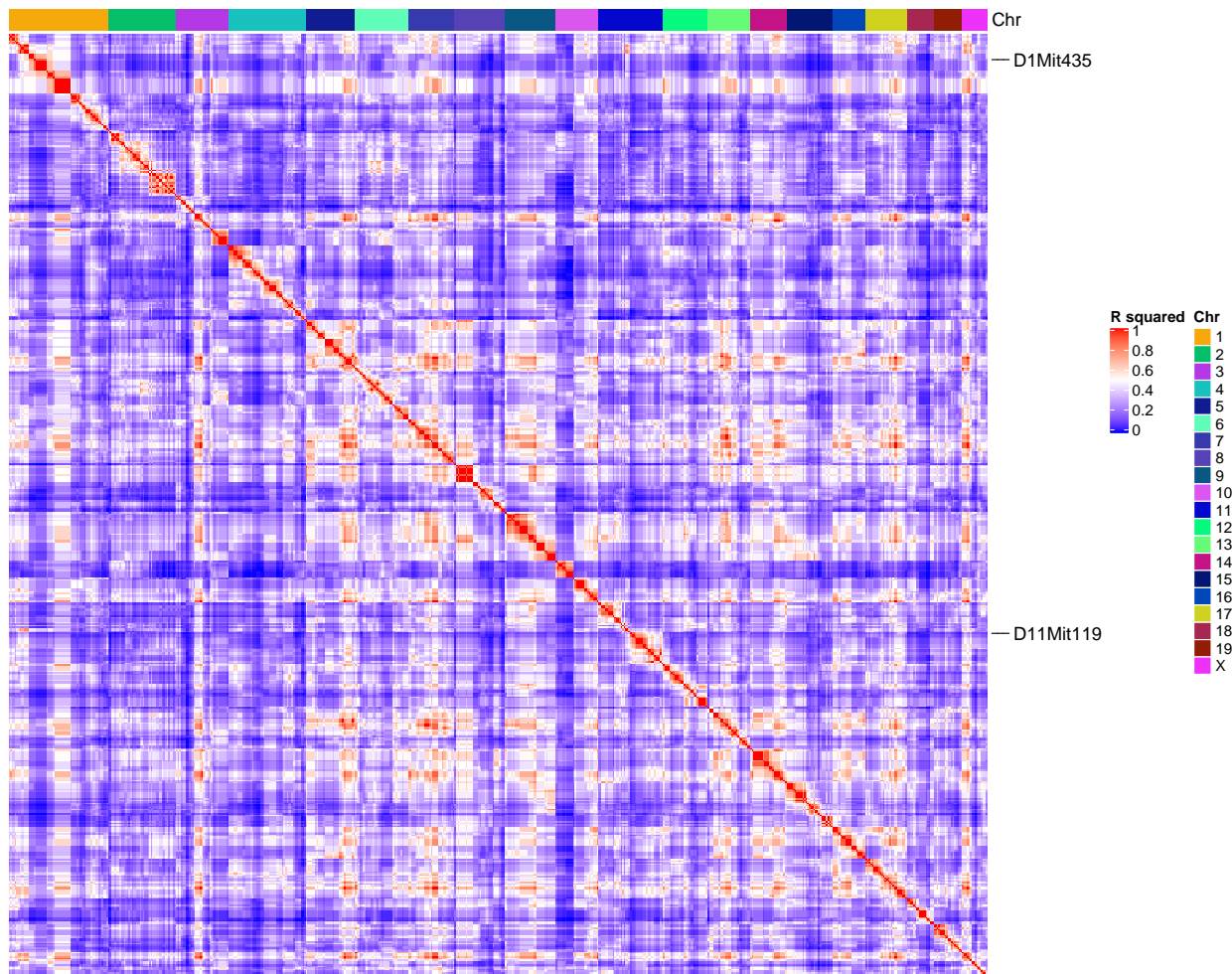


Figure B.3: LD structure among the markers in the mouse dataset

819 C ggmix Package Showcase

820 In this section we briefly introduce the freely available and open source `ggmix` package in R.
 821 More comprehensive documentation is available at <https://sahirbhatnagar.com/ggmix>.
 822 Note that this entire section is reproducible; the code and text are combined in an `.Rnw`¹ file
 823 and compiled using `knitr` [66].

824 C.1 Installation

825 The package can be installed from [GitHub](#) via

```
install.packages("pacman")
pacman::p_load_gh('sahirbhatnagar/ggmix')
```

826 To showcase the main functions in `ggmix`, we will use the simulated data which ships with
 827 the package and can be loaded via:

```
## library(ggmix)
data("admixed")
names(admixed)

## [1] "ytrain"      "ytune"        "ytest"        "xtrain"
## [5] "xtune"        "xtest"        "xtrain_lasso" "xtune_lasso"
## [9] "xtest_lasso"  "Xkinship"     "kin_train"    "kin_tune_train"
## [13] "kin_test_train" "mu_train"     "causal"       "beta"
## [17] "not_causal"   "kinship"     "coancestry"  "PC"
## [21] "subpops"
```

828 For details on how this data was simulated, see `help(admixed)`.

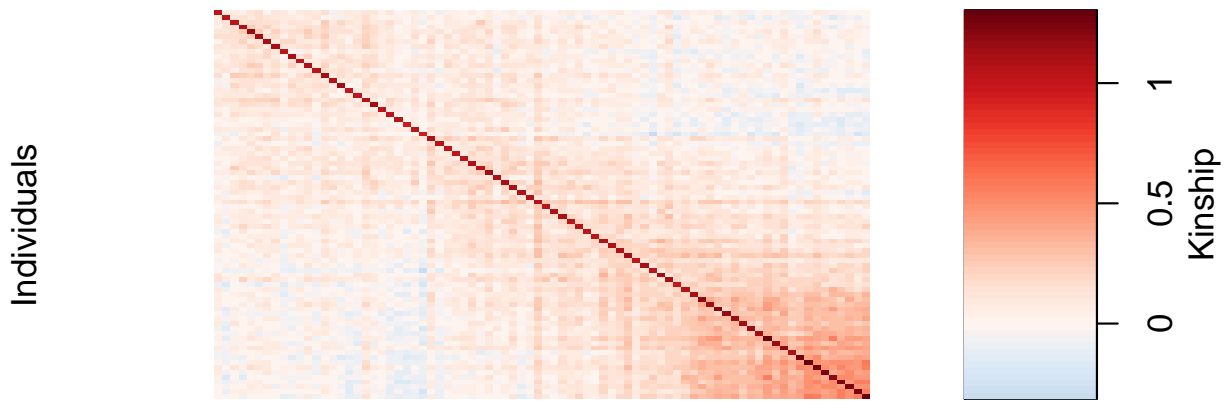
829 There are three basic inputs that `ggmix` needs:

- 830 1. Y : a continuous response variable
- 831 2. X : a matrix of covariates of dimension $N \times p$ where N is the sample size and p is the
 832 number of covariates
- 833 3. Φ : a kinship matrix

¹scripts available at <https://github.com/sahirbhatnagar/ggmix/tree/pgen/manuscript>

834 We can visualize the kinship matrix in the `admixed` data using the `popkin` package:

```
# need to install the package if you don't have it
# pacman::p_load_gh('StoreyLab/popkin')
popkin::plot_popkin(admixed$kin_train)
```



835

836 C.2 Fit the linear mixed model with Lasso Penalty

837 We will use the most basic call to the main function of this package, which is called `ggmix`.

838 This function will by default fit a L_1 penalized linear mixed model (LMM) for 100 distinct

839 values of the tuning parameter λ . It will choose its own sequence:

```
fit <- ggmix(x = admixed$xtrain,
```

```

y = admixed$ytrain,
kinship = admixed$kin_train)

names(fit)

## [1] "result"      "ggmix_object"  "n_design"     "p_design"     "lambda"
## [6] "coef"        "b0"          "beta"        "df"          "eta"
## [11] "sigma2"       "nlambda"      "cov_names"    "call"

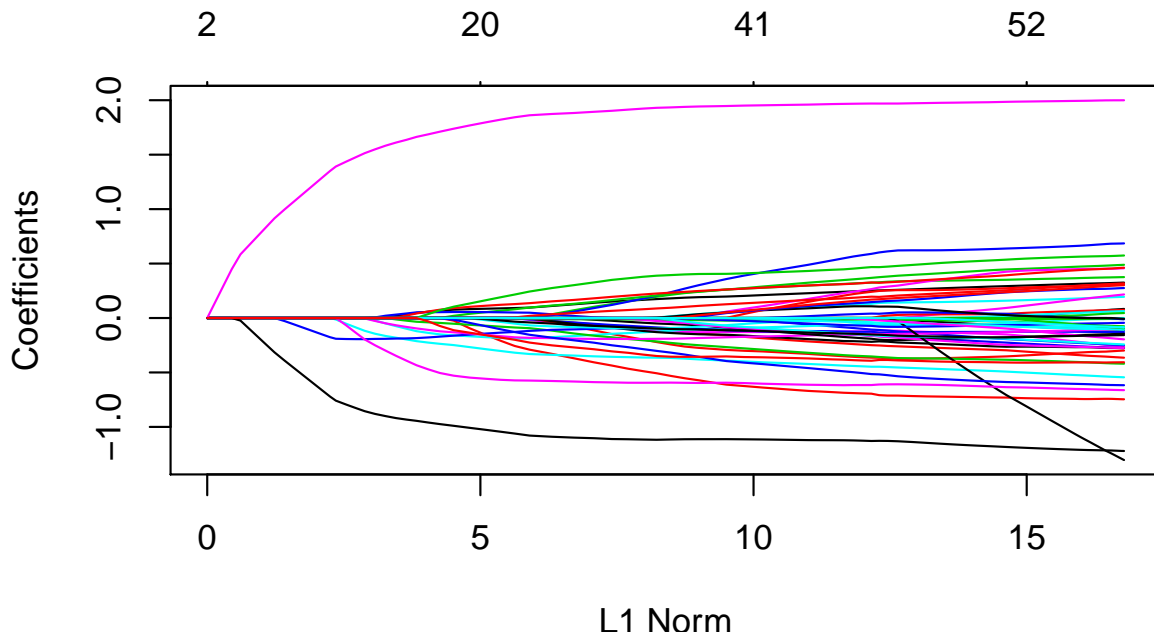
class(fit)

## [1] "lassofullrank" "ggmix_fit"

```

- 840 We can see the solution path for each variable by calling the `plot` method for objects of
 841 class `ggmix_fit`:

```
plot(fit)
```



842

- 843 We can also get the coefficients for given value(s) of lambda using the `coef` method for
 844 objects of class `ggmix_fit`:

```
# only the first 5 coefficients printed here for brevity
```

```

coef(fit, s = c(0.1,0.02))[1:5, ]

## 5 x 2 Matrix of class "dgeMatrix"
##           1         2
## (Intercept) -0.03715135  0.247105426
## X23        0.00000000  0.098030248
## X36        0.00000000 -0.013022250
## X38        0.00000000  0.005378361
## X40        0.00000000  0.004028934

```

845 Here, `s` specifies the value(s) of λ at which the extraction is made. The function uses linear
 846 interpolation to make predictions for values of `s` that do not coincide with the lambda
 847 sequence used in the fitting algorithm.

848 We can also get predictions ($X\hat{\beta}$) using the `predict` method for objects of class `ggmix_fit`:

```

# need to provide x to the predict function
# predict for the first 5 subjects
predict(fit, s = c(0.1,0.02), newx = admixed$xtest[1:5,])

##           1         2
## id26   2.30208546  2.45597763
## id39   0.87334032  1.62931898
## id45  -0.12296837 -0.06075786
## id52  -0.03715135 -0.97519671
## id53  -0.21046107 -0.23151040

```

849 C.3 Find the Optimal Value of the Tuning Parameter

850 We use the Generalized Information Criterion (GIC) to select the optimal value for λ . The
 851 default is $a_n = \log(\log(n)) * \log(p)$ which corresponds to a high-dimensional BIC (HD-
 852 BIC):

```

# pass the fitted object from ggmix to the gic function:
hdbic <- gic(fit)
class(hdbic)

## [1] "ggmix_gic"      "lassofullrank" "ggmix_fit"

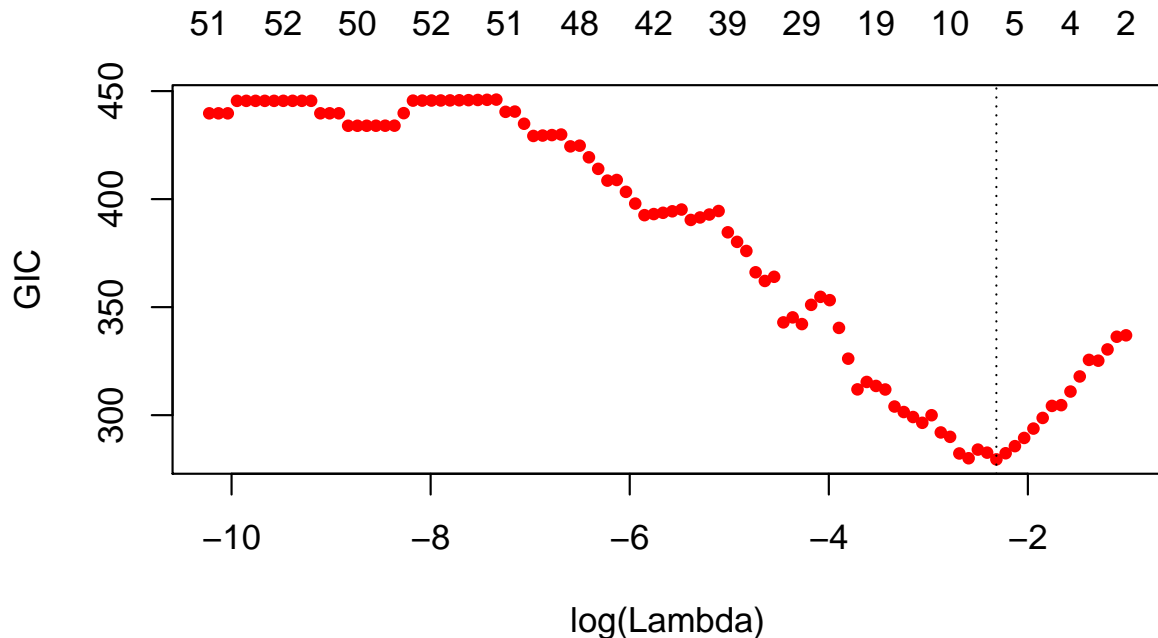
# we can also fit the BIC by specifying the an argument
bicfit <- gic(fit, an = log(length(admixed$ytrain)))

```

853 We can plot the HDBIC values against $\log(\lambda)$ using the `plot` method for objects of class

854 `ggmix_gic`:

```
plot(hdbic)
```



855 The optimal value for λ according to the HDBIC, i.e., the λ that leads to the minium HDBIC

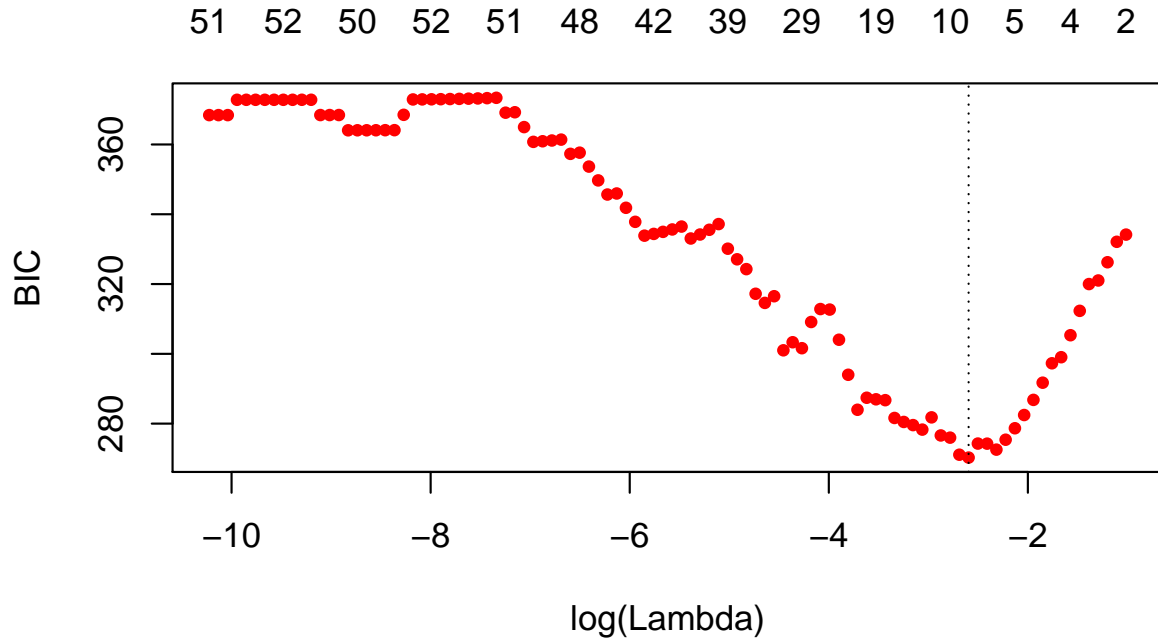
856 is:

```
hdbic[["lambda.min"]]
```

```
## [1] 0.09862269
```

858 We can also plot the BIC results:

```
plot(bicfit, ylab = "BIC")
```



859

```
bicfit[["lambda.min"]]
## [1] 0.07460445
```

860 C.4 Get Coefficients Corresponding to Optimal Model

861 We can use the object outputted by the `gic` function to extract the coefficients corresponding
 862 to the selected model using the `coef` method for objects of class `ggmix_gic`:

```
coef(hdbic)[1:5, , drop = FALSE]
## 5 x 1 sparse Matrix of class "dgCMatrix"
##           1
## (Intercept) -0.03660806
## X23         .
## X36         .
## X38         .
## X40         .
```

863 We can also extract just the nonzero coefficients which also provide the estimated variance
 864 components η and σ^2 :

```
coef(hdbic, type = "nonzero")

##           1
## (Intercept) -0.03660806
## X302       -0.17607392
## X524        1.34951500
## X538       -0.72052613
## eta         0.99000000
## sigma2      1.60476289
```

- 865 We can also make predictions from the `hdbic` object, which by default will use the model
 866 corresponding to the optimal tuning parameter:

```
predict(hdbic, newx = admixed$xtest[1:5,])

##           1
## id26   2.31027410
## id39   0.86922183
## id45  -0.12814532
## id52  -0.03660806
## id53  -0.21268198
```

867 C.5 Extracting Random Effects

- 868 The user can compute the random effects using the provided `ranef` method for objects of
 869 class `ggmix_gic`. This command will compute the estimated random effects for each subject
 870 using the parameters of the selected model:

```
ranef(hdbic)[1:5]

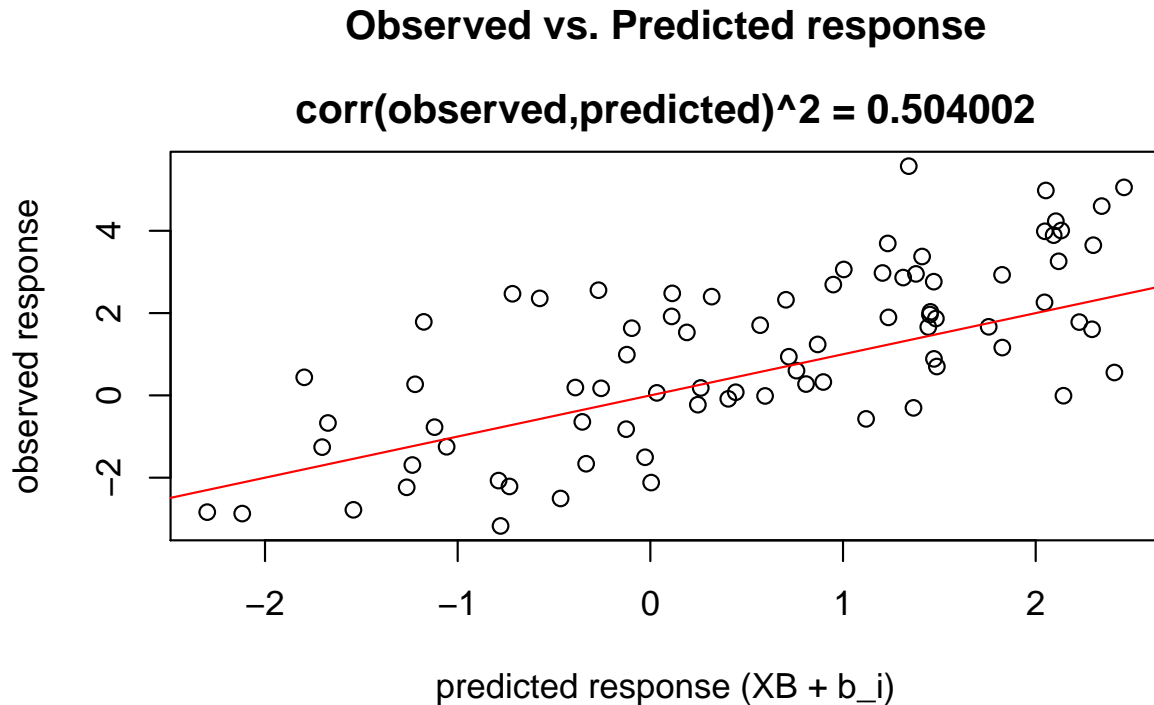
## [1] -2.4889655  1.1834200 -0.5641832 -0.9310334 -0.3458703
```

871 C.6 Diagnostic Plots

- 872 We can also plot some standard diagnostic plots such as the observed vs. predicted response,
 873 QQ-plots of the residuals and random effects and the Tukey-Anscombe plot. These can be
 874 plotted using the `plot` method on a `ggmix_gic` object as shown below.

875 C.6.1 Observed vs. Predicted Response

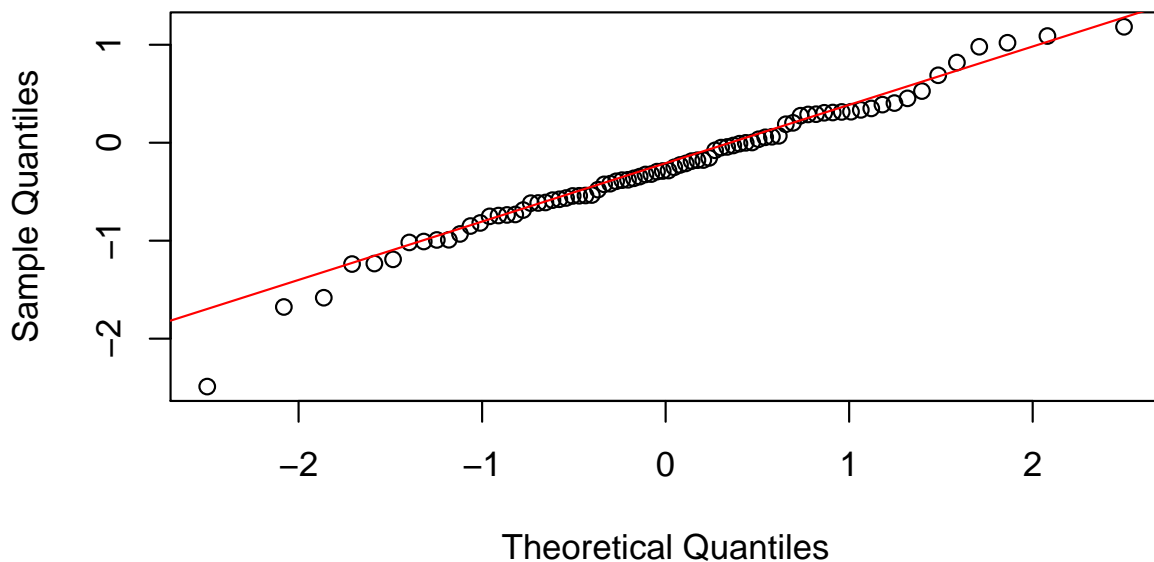
```
plot(hdbic, type = "predicted", newx = admixed$xtrain, newy = admixed$ytrain)
```



876

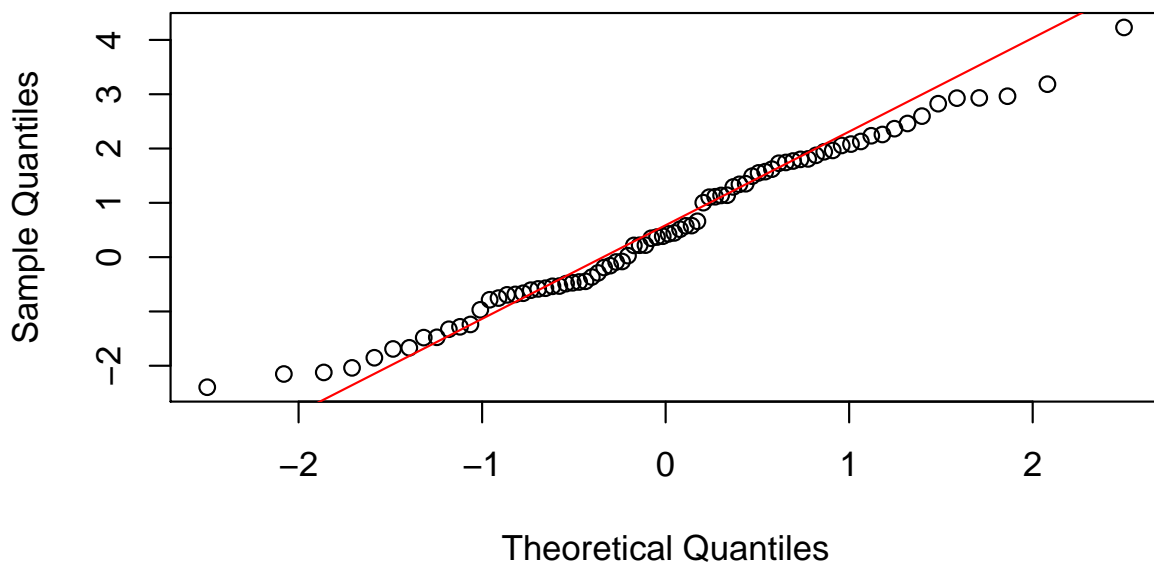
877 C.6.2 QQ-plots for Residuals and Random Effects

```
plot(hdbic, type = "QQranef", newx = admixed$xtrain, newy = admixed$ytrain)
```

QQ-Plot of the random effects at lambda = 0.10

878

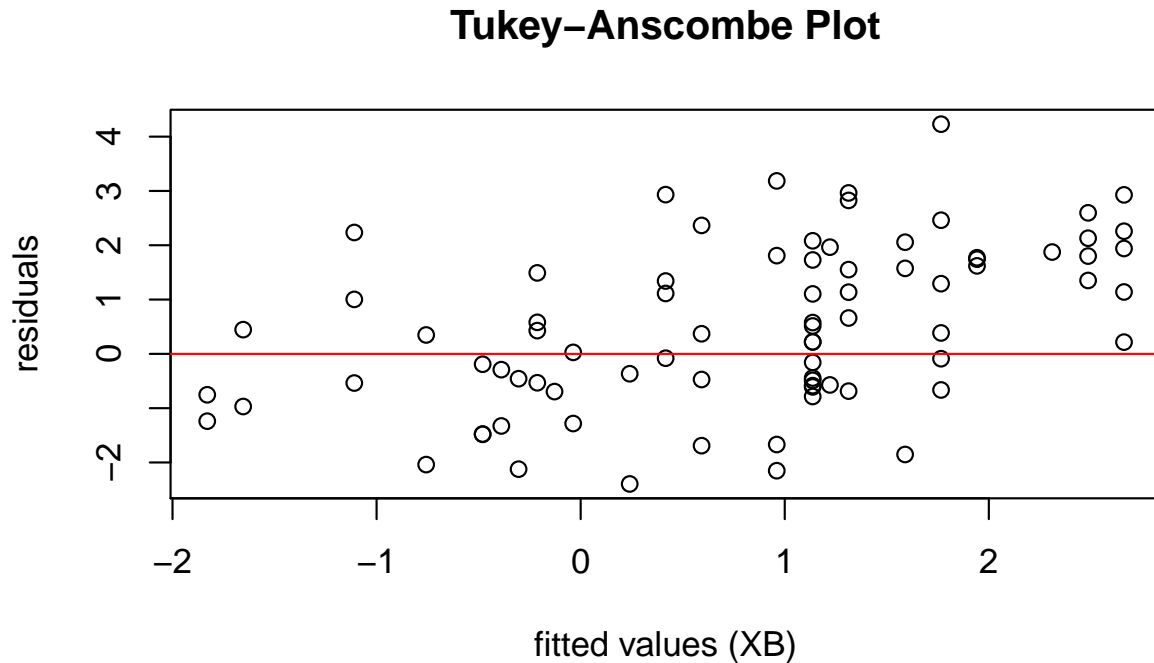
```
plot(hdbic, type = "QQresid", newx = admixed$xtrain, newy = admixed$ytrain)
```

QQ-Plot of the residuals at lambda = 0.10

879

880 C.6.3 Tukey-Anscombe Plot

```
plot(hdbic, type = "Tukey", newx = admixed$xtrain, newy = admixed$ytrain)
```



881